Enrichment of *SARM1* alleles encoding variants with constitutively hyperactive NADase in patients with ALS and other motor nerve disorders

Jonathan Gilley [1], Oscar Jackson [1], Menelaos Pipis [2], Mehrdad A. Estiar [3,4], Ziv Gan-Or [3,4,5], Stephen A. Goutman [6], Matthew B. Harms [7], Julia Kaye [8], Leandro Lima [8], Queen Square Genomics [2], John Ravits [9], Guy A. Rouleau [3,4,5], Stephan Züchner [10], Mary M. Reilly [2] and Michael P. Coleman [1†].

[1] John van Geest Centre for Brain Repair, Department of Clinical Neurosciences, University of Cambridge, Forvie Site, Robinson Way, Cambridge, CB2 0PY, UK
[2] Department of Neuromuscular Disease, UCL Queen Square Institute of Neurology and The National Hospital for Neurology, London, WC1N 3BG, UK
[3] Department of Human Genetics, McGill University, Montreal, H3A 1A1, Canada
[4] The Neuro (Montreal Neurological Institute-Hospital), McGill University, Montreal, H3A 2B4, Canada
[5] Department of Neurology and Neurosurgery, McGill University, Montreal, H3A 1A1, Canada
[6] Department of Neurology, University of Michigan, Ann Arbor, MI, USA
[7] Institute for Genomic Medicine, Columbia University, New York, NY100332, USA
[8] Finkbeiner lab, Center for Systems and Therapeutics, Bioinformatics Core, Institute of Data Science and Biotechnology, Gladstone Institutes, 1650 Owens Street, San Francisco, CA 94158, USA
[9] Department of Neurosciences, University of California, San Diego, La Jolla, CA92093, USA
[10] Dr. John T. Macdonald Foundation Department of Human Genetics and John P. Hussman Institute for Human Genomics, University of Miami Miller School of Medicine, Miami, FL, USA

Correspondence to:
[†] Prof Michael Coleman Email: mc469@cam.ac.uk
Dr Jonathan Gilley Email: jg792@cam.ac.uk
[†] Lead contact

ABSTRACT

SARM1, a protein with critical NADase activity, is a central executioner in a conserved programme of axon degeneration. We describe eight rare missense or in-frame microdeletion human *SARM1* variant alleles, in patients with amyotrophic lateral sclerosis (ALS), hereditary spastic paraparesis (HSP), or other motor nerve disorders, that alter the SARM1 auto-inhibitory ARM domain and constitutively hyperactivate SARM1 NADase activity. The constitutive NADase activities of six of the variants are at least as high as that of SARM1 lacking the entire ARM domain and greatly exceed the basal activity of wild-type SARM1, even in the presence of nicotinamide mononucleotide (NMN), its physiological activator. This rise in constitutive activity alone is enough to promote neuronal degeneration in response to otherwise non-harmful mild stress. Importantly, we provide evidence that these gain-of-function alleles are enriched in ALS and HSP patients compared to matched individuals without these conditions within ALS and other motor nerve disorder databases. Together, these data suggest these are risk alleles for ALS and other motor nerve disorders. The broad phenotypic heterogeneity and variable age-of-onset in patients with these alleles raises intriguing questions about the pathogenic mechanism of hyperactive SARM1 variants.

INTRODUCTION

The toll-like receptor adaptor protein SARM1 is required for axon degeneration after injury, in response to toxins and other insults, and in several models of neurodegenerative disease (Conforti et al., 2014; Coleman & Höke, 2020). In many of these situations the intimate interplay between pro-degenerative SARM1 (sterile alpha and TIR motif containing protein 1) (Osterloh et al., 2012; Gerdts et al., 2013) and its upstream, pro-survival regulator NMNAT2 (nicotinamide mononucleotide adenylyltransferase 2) (Gilley & Coleman, 2010; Gilley et al., 2015) is critical and most likely involves a disruption to normal nicotinamide adenine dinucleotide (NAD^+) homeostasis (Gerdts et al., 2016; Figley & DiAntonio, 2020). NMNAT2 is one of three NMNAT isoforms that catalyse the last step in NAD^+ biosynthesis and is the predominant NMNAT in axons. The SARM1 TIR domain has a critical NAD^+ consuming multifunctional glycohydrolase (NADase) activity (Essuman et al., 2017; Horsefield et al., 2019; Wan et al., 2019) and, intriguingly, NMNAT substrate, NMN, and its product, NAD^+, can both influence this activity: NMN activates SARM1 NADase by binding to an allosteric site in the auto-inhibitory ARM domain of the enzyme (Zhao et al., 2019; Figley et al., 2021), whereas NAD^+ can oppose this activation by competing for binding to the same site (Jiang et al., 2020; Sporny et al., 2020; Figley et al., 2021). Rising NMN and declining NAD^+ as a consequence of loss of very short-lived NMNAT2 in damaged axons (M. Di Stefano et al., 2015) thus leads directly to activation of SARM1 NADase and a self-reinforcing NAD^+ decline that represents one possible cause of degeneration.

As well as its established role in axons, SARM1 can promote neuronal cell death under certain conditions (Gerdts et al., 2013; Summers et al., 2014; Gerdts et al., 2015; Summers et al., 2016; Bratkowski et al., 2020), although to what extent the cell death and concurrent axon degeneration are primary or secondary events has not been determined. However, recent studies do suggest direct involvement of SARM1 in neuronal cell death in some situations, including photoreceptor loss in models of retinal degeneration and Leber congenital

amaurosis (LCA) (Ozaki et al., 2020; Sasaki et al., 2020) and as a result of Vacor neurotoxicity when specifically applied to cell bodies (Loreto et al., 2020).

Extensive evidence from animal models has implicated NMNAT-sensitive and SARM1-dependent axon degeneration and/or cell death in a variety of neurodegenerative disorders (Conforti et al., 2014; Coleman & Höke, 2020), but knowledge of genetic association with human diseases is more limited. To date, biallelic *NMNAT2* loss-of-function variants have been associated with two rare polyneuropathies that broadly resemble the corresponding mouse models (Gilley et al., 2013, 2019; Huppke et al., 2019; Lukacs et al., 2019), and *NMNAT1* mutations cause photoreceptor loss in LCA via a mechanism involving SARM1 (Sasaki et al., 2020). While no firm association between *SARM1* variation and human disease has yet been established, genome wide association studies (GWAS) have linked the *SARM1* chromosomal locus to sporadic ALS (Fogh et al., 2014; van Rheenen et al., 2016), although whether*SARM1* is the causative gene is not known.

Motor nerve disorders (MNDs) are neurodegenerative disorders that affect motor neurons in the brain, brainstem, and spinal cord. MNDs include ALS, the most common adult-onset MND, as well as other inherited conditions like HSP (Goutman, 2017). There is also some phenotypic and genetic overlap with the hereditary motor neuropathies (Rossor et al., 2012). These disorders exhibit broad phenotypic heterogeneity and variable age-of-onset. Recently, SARM1-dependent death mechanisms have been found to play a significant role in a mutant TDP-43 model of ALS (White et al., 2019). This is important as TDP-43 aggregation is an almost universal pathologic feature in ALS (Arai et al., 2006; Neumann et al., 2006). While removal of SARM1 does not alleviate motor neuron degeneration in a *SOD1* model of ALS (Peters et al., 2018), this could be explained by the finding that TDP-43 aggregation is not seen in ALS linked to *SOD1* or *FUS* mutations (Mackenzie et al., 2007; Maekawa et al., 2009; McAlary et al., 2019). It therefore remains possible that SARM1 plays an important role in a majority of ALS cases.

We used the Project MinE initiative (Project MinE ALS Sequencing Consortium, 2018), which includes whole genome sequencing (WGS) from several thousand ALS patients and

non-ALS controls to identify potential associations between *SARM1* genetic variation and the disease. We identified a number of rare alleles specific to ALS patients in this cohort encoding missense substitutions and in-frame microdeletions in the auto-inhibitory ARM domain of SARM1 and found that these dramatically increase constitutive NADase activity to a level substantially higher than wild-type SARM1, even after its activation by NMN. We subsequently found one of these alleles in independent ALS and HSP cohorts, along with a new, rare gain-of-function allele that was also present in a patient with a slowly progressive upper and lower motor nerve disorder. We propose that these alleles are thus strong candidate risk factors for ALS and other MNDs. During these studies, a preprint manuscript reported low NAD^+ levels in neurons overexpressing SARM1 variants from ALS patients and a neurodegenerative phenotype of one when overexpressed in mice (Bloom et al., 2021).

RESULTS

Identification of a cluster of patient-specific SARM1 ARM domain coding variants in Project MinE

Project MinE consortium Data Freeze 1 (DF1) contains WGS data for 4,366 mostly sporadic ALS patients and 1,832 non-ALS controls. Here, we noted an uneven distribution of mostly rare missense single nucleotide polymorphisms (SNPs) and small, in-frame deletions between the patient and control groups in the *SARM1* gene (Figure 1). To determine the burden of *SARM1* variants between ALS patients and controls, we took an unbiased approach. We analysed all rare variants (minor allele frequency, MAF < 0.01) at both the entire gene level and domain-by-domain. While *SARM1* appears unremarkable at the entire gene level (burden test p=0.49, SKAT-O p=0.63), there was a clear association with ALS in the ARM domain (burden test p=0.005, SKAT-O p=0.017, after false discovery rate correction) but not in the SAM and TIR domains (p>0.3 for both). This is consistent with gain-of-function (GoF) for this prodegenerative protein being more likely to result from disruption of its inhibitory ARM domain than its SAM or TIR domains. In particular, of the 16 coding variants in the ARM domain region spanning amino acids 112 to 385 of the canonical 724 amino acid SARM1 protein, all are seen in patients but only the two relatively more common variants are also seen in controls (Table 1). In contrast, no variants within this region are only seen in controls. Furthermore, where the MAF for an allele is known, the number of allele counts in the patient group is higher than expected for almost all of the patient-specific alleles in this region, whereas the two alleles present in both patient and control groups are seen at close to the expected number of times in each group based on their MAFs (Table 1).

Given the importance of the ARM domain in auto-inhibition of SARM1 activity and its pro-degenerative function, we hypothesised that the unusual cluster of enriched patient-specific SARM1 ARM domain coding variants in Project MinE could thus represent risk alleles for ALS through GoF. In contrast, we hypothesised that those alleles with matched frequency in patient and control groups would be expected not to substantially alter SARM1 function.

Several ALS patient-specific SARM1 ARM domain coding variants in Project MinE increase NAD^+ depletion in transfected HEK cells

As an initial screen to identify potential GoF for the proteins encoded by the ARM domain *SARM1* variant alleles, we assessed NAD^+ depletion in HEK 293T cells transfected with expression constructs for WT or variant SARM1. Conditions were optimised to detect both GoF and loss-of-function (LoF) (Supplementary Figure 1). NAD^+ levels in cell extracts were approximately halved with WT SARM1 (as a result of overexpression of a low basal activity) but we observed a substantially greater lowering of NAD^+ for six of the ALS-specific variants - L223P, Δ226-232, Δ249-252, V331E, E340K and T385A SARM1 - suggestive of strong NADase GoF (Figure 2A). Smaller, but still statistically significant lowering of NAD^+ was also seen for a further three variants - V112I, A275V and A341V SARM1 - suggestive of more modest GoF. In contrast, the other patient-specific variants and the two variants showing similar prevalence in ALS patients and controls all affected NAD^+ levels to a similar extent as WT SARM1. The strongest putative GoF variants also lowered ATP levels (Figure 2B), with ATP loss thus likely to be a lagging consequence of the more substantial depletion of NAD^+, and also lowered $NADP^+$, an alternative substrate of SARM1 glycohydrolase activity (Essuman et al., 2018; Horsefield et al., 2019; Wan et al., 2019), to a greater extent than WT SARM1 (Figure 2C).

Importantly, increased NAD^+ depletion in these assays is not a result of increased variant expression. In fact, the putative strong GoF variants were barely detectable by immunoblotting using conditions that allowed easy detection of WT SARM1 (Figure 2D). These variants thus achieve greater NAD^+ depletion despite much lower expression levels, further reinforcing their GoF credentials. Levels of ZsGreen, a fluorescent protein co-expressed with SARM1 from a bicistronic cassette, also appeared substantially lower in the extracts of cells transfected with the putative strong GoF variants (Figure 2D). Fluorescence imaging suggested that this predominantly reflects a global suppression of ZsGreen levels within cells rather than reduced transfection efficiency (Figure 2E) and overall NAD^+ depletion

of more than 90% by the putative strong GoF variants would anyhow appear incompatible with lower transfection rates. We therefore propose that vector-driven expression of ZsGreen, and possibly also SARM1 itself, is acutely sensitive to cellular NAD^+ and ATP levels. In contrast to previous reports (Panneerselvam et al., 2012; Gerdts et al., 2013; Sporny et al., 2019, 2020) we also did not see any obvious change in HEK cell morphology suggestive of any loss of cell viability in our assays (Figure 2E). However, we had previously found that constitutively hyperactive SARM1 lacking the entire auto-inhibitory ARM domain (SAM-TIR, amino acids 409-724) caused cell death in a highly cell density-dependent manner and caused minimal loss of viability at the cell density used in our assays (Supplementary Figure 2).

Last, we tested the effects of co-expression of a strong GoF variant with WT SARM1 in HEK cells to partially mimic heterozygosity in the ALS patients. For this purpose, we chose Δ226-232 SARM1 as it is present in more than one patient in Project MinE. We found that NAD^+ depletion in cells co-transfected with equal amounts of the Δ226-232 and WT SARM1 expression constructs was similar to that in cells transfected with the Δ226-232 SARM1 construct alone (Figure 3A) and ZsGreen expression was also strongly suppressed in both situations (Figure 3B). Interestingly, expression of (HA-tagged) WT SARM1 was also substantially suppressed when co-expressed with (Flag-tagged) Δ226-232 SARM1 compared to when co-expressed with (Flag-tagged) WT SARM1 (Figure 3B). Together, these data suggest that the strong GoF effects of Δ226-232 SARM1 are dominant in cells.

The ALS patient-specific SARM1 GoF variants in Project MinE have very high constitutive NADase activity

Measurements of NAD^+ levels in transfected HEK cells indirectly pointed to variable degrees of NADase GoF for a number of the Project MinE patient-specific SARM1 ARM domain coding variants. Therefore, we next directly tested the NADase activity of WT SARM1 and SARM1 variants after purification from HEK293 cell lysates by immunoprecipitation. Nicotinamide riboside (NR), a cell permeable NAD^+ precursor, was also added to the HEK cells to boost

NAD^+ biosynthesis and improve the yield of immunoprecipitated proteins, particularly the strong GoF variants (Supplementary Figure 3).

Constitutive (basal) NADase activity of the purified proteins in reactions containing just NAD^+ was assayed first. We calculated an NAD^+ consumption rate of 0.93 ±0.16 mol/min/mol enzyme for WT SARM1, which is comparable to a previously reported rate of 1.16 ±0.26 mol/min/mol enzyme (Zhao et al., 2019), but found strikingly increased rates for the presumed GoF variants: rates were around 20 times higher for five of the ALS patient-specific variants - L223P (20.41 ±2.25 mol/min/mol enzyme), Δ226-232 (19.29 ±2.12 mol/min/mol enzyme), Δ249-252 (19.33 ±2.27 mol/min/mol enzyme), V331E (18.30 ±1.04 mol/min/mol enzyme) and E340K (21.04 ±2.78 mol/min/mol enzyme) - and around 10 times higher for a sixth - T385A (10.69 ±0.75 mol/min/mol enzyme) (Figure 4A). These activities are consistent with them having the strongest effects on metabolites in the HEK cell assays above. However, the degree to which their activities are higher than WT SARM1 was unexpected given the rates are similar to, or even slightly higher than a rate of 14.98 ±4.91 mol/min/mol enzyme calculated from separate purifications of constitutively active SAM-TIR. Of the three variants, V112I, A275V and A341V SARM1, that had more modest effects on cellular NAD^+ levels in transfected HEKs, V112I SARM1 had a rate twice as high as WT SARM1 (at 2.13 ±0.20 mol/min/mol enzyme), whereas a marginal increase in measured activity of A275V SARM1 was not significant and activity of A341V SARM1 was similar to that of WT SARM1 Figure 4A). Interestingly, the basal NADase rates calculated for P332Q and N337D, the variants present in both the patient and control groups, and R310H, a patient-specific variant, suggested partial LoF (Figure 4A).

ALS patient-specific SARM1 variants with high constitutive NADase activity showed no further activation by NMN

The NADase activity of full-length SARM1 can be induced by NMN (Zhao et al., 2019; Loreto et al., 2020; Figley et al., 2021), a regulatory control mechanism that appears to play a critical

role in axon degeneration (M. Di Stefano et al., 2015; Michele Di Stefano et al., 2017). Greater activation by NMN could thus represent an alternative pro-degenerative GoF mechanism. We therefore additionally tested the immunoprecipitated ARM domain coding variants for NMN-dependent triggering of their NADase activity.

We first assessed activation by 50 μM NMN. This provided robust activation, roughly tripling the NADase activity of WT SARM1 (Figure 4B). In contrast, the high constitutive activity of all six strong GoF variants in this assay - L223P, Δ226-232, Δ249-252, V331E, E340K and T385A SARM1 - were not further induced (Figure 4B). With the exception of V112I, which was not induced above its already moderately raised constitutive activity, all other variants were NMN-inducible to some extent, and most showed levels of inducibility similar to WT SARM1 (Figure 4B and Supplementary Figure 4A and 4C). Intriguingly, activity of the P332Q SARM1, a variant equally abundant in ALS patients and controls, appeared much more inducible than WT SARM1 (Supplementary Figure 4C), but this largely appeared to be a reflection of its substantially lower basal activity and its activated rate was only marginally higher than that of WT SARM1 (Figure 4B and Supplementary Figure 4A). Indeed, none of the NMN-activated rates of any of the other NMN-responsive variants were significantly higher than that of WT SARM1, and for some (R244S, R310H and N337D SARM1) the activated rate was lower (Figure 4B and Supplementary Figure 4A).

Increased sensitivity to lower concentrations of NMN, closer to the activation threshold, could also represent a pro-degenerative GoF mechanism so we next assessed triggering of NADase activity by 10 μM NMN for all but the strong GoF variants. The increase in activity of WT SARM1 in the presence of 10 μM NMN was roughly half that seen with 50 μM NMN (in parallel assays) and all the ALS patient variants previously found to be responsive to 50 μM NMN showed a similar or even lower relative level of activation with 10 μM NMN (Figure 4C and Supplementary Figure 4B and 4D), with the exception of R310H SARM1 which instead showed equally low activation at both NMN concentrations (Figure 4C). As with 50 μM NMN, 10 μM NMN induced P332Q SARM1 activity to a greater extent than that of WT SARM1

(Supplementary Figure 4D) but its activated rate in the presence of 10 μM NMN in this case was below that of WT SARM1 (Figure 4C and Supplementary Figure 4B).

Together, these NADase activity data indicate that GoF among the SARM1 ALS patient-specific variants involves greatly enhanced constitutive (basal) activity and not enhanced responsiveness to its activator NMN. Indeed, none of the seven variants with raised constitutive activity show any clear triggering by NMN in this assay. While these data also suggest that a number of the *SARM1* alleles that appear only in the patient group in Project MinE encode variants that are neutral or even partial LoF with respect to NADase activity, this could, in part, simply reflect a greater chance of appearing there than in the smaller control group. Additionally, despite causing moderate depletion of NAD^+ in transfected HEK cells, NADase activity data suggests that A275V SARM1 is, at best, a very modest GoF and A341V SARM1 has properties comparable to WT SARM1. However, we cannot rule out GoF for these variants under physiological conditions.

Acute expression of strong GoF Δ226-232 SARM1 reduces viability of sympathetic neurons under stress conditions

To test the effects of greatly enhanced constitutive activity in neurons, we used an established method involving microinjection of controlled amounts of expression constructs into cultured sympathetic neurons from the superior cervical ganglion (SCG neurons), a neuronal subtype very amenable to this approach (Gilley & Loreto, 2020). The amount of SARM1 expression vector injected was minimised in order to reduce possible artefactual effects of high overexpression. While exogenous WT SARM1 is essentially undetectable by immunostaining under these conditions, it is enough to restore injury-induced neurite degeneration of injected *Sarm1*$^{-/-}$ neurons (Supplementary Figure 5) indicating a low but functionally-relevant expression level. A DsRed expression construct was co-injected for clear visualisation of the injected neurons and their neurites.

We first compared the effects of Δ226-232 SARM1, as a representative strong GoF variant, with those of WT SARM1 in wild-type SCG neurons. Δ226-232 SARM1 was thus expressed alongside endogenous (WT) SARM1 as in individuals heterozygous for the variant, although with higher overall SARM1 levels than in the physiological setting. We consistently saw substantially fewer DsRed labelled neurons 24 h after injection with the Δ226-232 SARM1 construct compared to the WT SARM1 construct and the intensity of DsRed in the few labelled neurons was also reduced (Figure 5A and 5B). This likely reflected robust suppression of DsRed expression in the presence of Δ226-232 SARM1, analogous to the suppression of ZsGreen in transfected HEK cells (Figure 2D and 2E). However, this severely limited our ability to assess neuron / neurite survival, so we could not rule out an additional reduction in neuronal viability in this situation.

NR can substantially increase ZsGreen levels in HEK cells overexpressing NADase-competent WT or SAM-TIR SARM1 (Supplementary Figure 3A and 3B) and we similarly found that NR treatment also boosted DsRed expression in injected neurons (Figure 5A and 5B). This greatly improved the visualisation of the injected neurons and their neurites, enabling us to next assess their response to various stresses. Intriguingly, we found that the modest stress relating to sudden changes in culture conditions associated with a media change, even to new NR-containing media, was sufficient to trigger a substantial loss of neurons injected with the Δ226-232 SARM1 expression construct (compared to not changing media) (Figure 5C and 5D). In contrast, neurons injected with the WT SARM1 construct were unaffected. Furthermore, additional manipulations designed to reduce NAD^+ biosynthesis - removal of NR, or a combination of NR removal and incubation with NAMPT inhibitor FK866 to block the rate-limiting step in the NAD^+ salvage pathway - caused additional, incremental decreases in cell survival on top of the effect of media change (Figure 5C and 5D). Expression of Δ226-232 SARM1 in the presence of endogenous WT SARM1 thus greatly increases the sensitivity of cultured SCG neurons to quite modest stress and this is, at least in part, likely the result of compromised NAD^+ homeostasis. Importantly, we could not differentiate the timing of cell

death and neurite degeneration in these experiments suggesting that either the primary effect is on neuronal viability or that separate cell body and neurite death mechanisms occur simultaneously.

Identification of an additional *SARM1* GoF allele and patient association of *SARM1* GoF alleles in other databases

Subsequent to the characterisation of the Project MinE variants, as described above, we found another rare ARM domain *SARM1* variant allele, encoding R267W SARM1, in a patient with an upper and lower motor nerve disorder (UCL cohort, see below). We found that R267W SARM1 depletes NAD^+ in HEK cells as robustly as Δ226-232 SARM1, indicative of similarly very high constitutive NADase activity (Figure 6), thereby identifying R267W SARM1 as another strong GoF variant.

Having thus identified a total of eight different *SARM1* alleles encoding SARM1 variants with confirmed or probable NADase GoF, we next asked whether any of these alleles were specifically seen in patients in two other independent motor nerve disorder databases, the Answer ALS project database (Rothstein, 2020) and the GENESIS database (Gonzalez et al., 2015). We found four further occurrences of patients heterozygous for the Δ226-232 or R267W *SARM1* alleles in these databases, three of them ALS patients (two Δ226-232 and one R267W) and the other an HSP patient (Δ226-232) (Table 1). Importantly, as in Project MinE, there were no occurrences of these alleles in the 11,694 non-ALS/HSP individuals in these additional databases. In Project MinE, the association of ARM domain variants with disease (see above) seems likely to have been largely driven by seven patient-specific GoF variants (V112I, L223P, Δ226-232, Δ249-252, V331E, E340K and T385A) in eight individuals. We therefore additionally tested the burden of all eight rare GoF variants (including R267W) in all three datasets (Project MinE, Answer ALS and GENESIS), and this revealed a highly significant association with disease (burden test and SKAT-O $p<0.0000014$), with 12 out of 7,056 ALS/HSP patients possessing *SARM1* GoF variant alleles versus none in 13,526 non-

ALS/HSP controls. Notably, enrichment in patients was also specifically suggested for the Δ226-232 *SARM1* variant when considered alone (5 in 7,056 ALS/HSP patients versus none in 13,526 non-ALS/HSP controls, p=0.0087, χ^2 test with Yates' correction).

Phenotypic heterogeneity and variable age-of-onset in patients with *SARM1* GoF alleles

Finally, we have collated clinical information for the majority of patients heterozygous for the Δ226-232 and R267W *SARM1* variant allele. These include the ALS and HSP patients with these alleles in Answer ALS and GENESIS, together with the additional R267W patient with an upper and motor nerve disorder (UCL cohort) and another Δ226-232 ALS patient from an independent source (not previously described) (Table 2). These data reveal a broad range of clinical presentation and a highly variable age-of-onset, with no obvious heritability. Notably, two of the ALS patients are also heterozygous for variant alleles in other genes previously associated with ALS or recessive Charcot-Marie-Tooth disease type 4J (CMT4J), although it is important to stress that these specific variant alleles may not be the sole cause of disease in these cases: the I114T *SOD1* variant (previously reported as I113T) shows incomplete penetrance (Lopate et al., 2010), while the L17P *FIG4* variant has previously only been associated with CMT4J when in combination with a null allele (Nicholson et al., 2011). However, it does raise the interesting possibility that the *SARM1* GoF alleles might interact with other risk alleles to enhance phenotypic expressivity in some cases and this could underlie some of the variability in clinical presentation.

DISCUSSION

Here, we have identified a total of eight *SARM1* variant alleles encoding SARM1 with constitutively raised NADase activities in patients with ALS or other MNDs with significant phenotypic heterogeneity with respect to age-of-onset, clinical presentation and severity. Crucially, these were seen at a higher frequency in disease cohorts than in the wider population and showed statistically significant enrichment in ALS/HSP patients. Surprisingly, in NADase assays of recombinant SARM1, six of the variants have constitutive NADase activity as much as ten to twenty times higher than the basal activity of WT SARM1. Another variant, which we identified later, likely has similarly high activity based on its ability to robustly deplete NAD^+ in HEK cells. Notably, these activities are substantially higher even than the activity of WT SARM1 activated by NMN, a natural activator of SARM1 NADase during injury-induced and other related forms of axon degeneration. Furthermore, we found that restricted and acute exogenous expression of a variant with high constitutive NADase activity (in the presence of endogenous SARM1) is sufficient to promote cell death (and simultaneous or secondary axon degeneration) in primary cultured neurons in response to otherwise non-harmful mild stress.

As SARM1 NADase activity has been implicated as a critical driver of axon degeneration and neuronal death, these strong NADase GoF *SARM1* alleles are thus candidate risk alleles for ALS and other MNDs, especially as the effect appears to be dominant. While the proportion of patients with *SARM1* GoF coding variants is <0.2%, this adds support for an involvement of other SARM1-dependent mechanisms in ALS. For example, we suggest the GWAS association between the human *SARM1* locus and ALS (Fogh et al., 2014; van Rheenen et al., 2016) could be driven by increased SARM1 expression. Reduced expression of Stathmin-2 (STMN2, also known as SCG10), which potentiates programmed axon degeneration (Shin et al., 2012), has also been linked to the disease. Specifically, STMN2 depletion increases the vulnerability of ALS patient iPSC-derived neurons (Klim et al., 2019; Melamed et al., 2019), and a non-coding *STMN2* variant that influences gene expression has recently also been

associated with increased risk of sporadic disease (Theunissen et al., 2021). Of course, it will be important to firmly establish the extent of the penetrance of the GoF alleles identified here and whether or not any show a familial association with MNDs. However, their apparent prevalence in sporadic cases, and co-occurrence with partially-penetrant disease variants of other genes in some patients, suggest they may have to interact with other risk factors to reveal their pathogenicity. Future human genetics studies should help to address these possible associations. There are also a number of drug development programmes and other avenues of therapeutic intervention targeting SARM1 currently being pursued (Geisler et al., 2019; Hughes et al., 2021; Bosanac et al., 2021) and individuals with GoF *SARM1* alleles would thus be ideal test subjects if other requirements are met.

Constitutive removal of NMNAT2 causes mice to die a birth with a severe SARM1-dependent axonal defect (Gilley et al., 2013, 2015), with a potentially even more severe outcome in humans (Lukacs et al., 2019). Clearly, though, chronic expression of constitutively hyperactive SARM1 variants, with NADase activity predicted to be substantially higher than NMN-triggered SARM1 resulting from NMNAT2 deficiency, is not as detrimental to axon (and/or neuron) survival as individuals with strong GoF *SARM1* alleles would otherwise also not survive beyond birth. We propose that this apparent discrepancy could be explained by compensatory changes triggered during development that are only associated with chronic expression of the much higher constitutive NADase activity. Suppressed SARM1 expression, as seen in transfected HEK cells, is one way that NADase activity could be kept in check, although this seems to be a global effect linked to low NAD^+ (and/or ATP) levels and it is hard to imagine long-term neuron survival under these conditions. In contrast, the loss of neuron viability seen in our SCG assays will be a consequence of acute overexpression (further boosted by NR) that would likely limit the impact of any compensatory changes, if they occur at all in such a short timeframe. Intriguingly, in this respect, we also observed differences between constitutive and acute silencing of a single *Nmnat2* allele suggestive of compensatory changes in the chronic condition (Gilley et al., 2013).

Recently, substantial progress has been made into elucidating the mechanism of auto-inhibition of SARM1 NADase activity by the ARM domain (Jiang et al., 2020; Sporny et al., 2020; Shen et al., 2021) and the strong GoF variants identified here represent useful tools for further understanding. Given their vastly higher activities relative to NMN-activated WT SARM1, it seems unlikely that the mutations simply mimic the effects of NMN binding and/or block NAD^+ binding in the allosteric site in the ARM domain. Consistent with this, there is overlap with residues that appear to be critical for NAD^+/NMN interactions (Figley et al., 2021). Our finding that the constitutive activities of the strong GoF variants are at least as high as that of the SAM-TIR protein lacking the entire auto-inhibitory ARM domain instead suggests that the amino acid changes that confer strong GoF, as reported here, probably cause more profound structural changes that disrupt inhibitory interaction between the ARM and TIR domains completely. This would also explain the non-responsiveness of the variants to NMN. Interestingly, some of the changes affect residues that appear to be located at an ARM-TIR interface (R249 and E252), and others at ARM-ARM and ARM-SAM interfaces (T385 and V331 respectively) (Shen et al., 2021).

Surprising to us, raised constitutive activity was the only GoF effect we identified among the ALS patient *SARM1* alleles. We found no GoF in relation to activation by NMN, either in terms of absolute NADase activity in the presence of high NMN, or sensitivity to lower NMN concentrations, both of which might be predicted to have significant pro-degenerative effects. While our attempts to identify alterations to NMN-responsiveness were thorough, some may only be revealed under very specific conditions in cells that our current assays do not mimic effectively. Intriguingly, P332Q SARM1, encoded by an allele with matched frequencies in patient and control groups that would thus be expected to have a neutral effect, actually showed a much greater degree of inducibility by NMN than WT SARM1. However, this largely reflected activation from a much lower basal activity and, while its NMN-induced NADase was marginally higher than WT SARM1 in the presence of 50 μM NMN, it was lower than WT SARM1 in the presence 10 μM NMN which may be closer to post-injury levels in axons. As such, we do not consider P332Q to be a pathogenic GoF substitution but further study could

nevertheless provide insight into NMN-triggering of SARM1 as P332 has so far not been implicated in NMN binding (Figley et al., 2021).

The non-responsiveness of the constitutively hyperactive ALS patient variants to NMN also raises questions about how axons of individuals heterozygous for the constitutive GoF variant alleles respond to stresses that normally trigger SARM1-dependent degeneration. If the wild-type SARM1 in these individuals, presumably complexed with GoF SARM1 in hetero-octamers, can still be activated by NMN, then the resulting increase in activity would likely be minimal relative to an already very high constitutive NADase activity contributed by the hyperactive NADase variant. Thus, it will be important to understand how constitutive SARM1 activity, rather than NMN-induced activity, may contribute to pathogenesis, and whether increased activation is important in other cases.

In summary, we report eight *SARM1* alleles with low MAFs that encode variants with increased basal NADase activity, the majority to a degree much higher than NMN-activated wild-type SARM1. This raises intriguing questions both about their potential pathogenic roles and about why this extraordinarily high NADase activity is not immediately lethal. There is also phenotypic heterogeneity in the clinical presentation, reminiscent of other ALS disease genes. Thus, while replication in other cohorts and direct evidence that SARM1 activity is necessary for pathogenesis will all be important to firmly establish causation, the elevated prevalence of these GoF alleles, specifically in ALS and other motor nerve disorder patients, strongly suggests that SARM1 is a risk factor in this group of diseases.

MATERIALS AND METHODS

Constructs and reagents

The bicistronic pLVX-IRES-ZsGreen1 vector (Takara Bio) was the backbone for all SARM1 expression constructs used in this study, unless stated otherwise. SARM1 and ZsGreen(1) are co-expressed from a bicistronic mRNA transcript under the control of the CMV promoter. The complete open reading frame (ORF) of the canonical 724 amino acid human SARM1 protein was cloned into the first cistron between the *Eco*RI and *Spe*I restriction sites. An in-frame Flag tag followed by a stop codon were introduced between the *Xba*I and *Bam*HI restriction sites immediately 3' to SARM1 ORF at the C-terminus. The expressed SARM1 thus possesses a C-terminal Flag (after a 4 amino acid linker). ZsGreen occupies the second cistron and undergoes IRES-driven translation. For experiments in Figure S5, untagged SARM1 was expressed from a pCMV-Tag4A vector backbone (Agilent Technologies) with the 724 amnio acid ORF, including a consensus Kozak sequence immediately 5' to the ATG codon and a stop codon at the 3' end of the ORF, cloned between the *Bam*HI and *Xho*I restriction sites of the multiple cloning site. Point mutations were introduced into constructs by QuikChangeII site-directed mutagenesis (Stratagene) and microdeletions were introduced using overlap extension PCR (J. Lee et al., 2010). The presence of the mutations and absence of other PCR errors was confirmed by DNA sequencing (Department of Biochemistry, University of Cambridge). pDsRed2-N1 (Clontech) was used for expression of variant *Discosoma* red fluorescent protein (DsRed) to label microinjected neurons and their neurites.

PBS without calcium and magnesium (Merck) was used throughout, unless stated otherwise. NAD^+ and NMN (both Merck) were dissolved in water and stored frozen as concentrated stocks. Nicotinamide riboside (NR) was prepared as a 100 mM stock from Tru Niagen® capsules by dissolving the contents in PBS and passing through a 0.22 µm filter. NAMPT inhibitor FK866 was a kind gift from Prof. Armando Genazzani, University of Novara.

HEK 293T culture and transfection

HEK 293T (clone 17) cells were originally obtained from the American Type Culture Collection (ATCC). Cells were grown in DMEM with 4,500 mg/L glucose and 110 mg/L sodium pyruvate (PAA), supplemented with 2 mM glutamine, 1% penicillin/streptomycin (both Invitrogen), and 10% fetal bovine serum (PAA). Cells at 50-70% confluence were transfected with expression constructs (as described in the text / figure legends) using Lipofectamine 2000 reagent (Invitrogen) according to the manufacturer's instructions. Amounts of DNA constructs transfected are described in applicable sections.

Measurements of nucleotide levels in transfected HEK 293T cell extracts

Transfected HEK cells (from individual wells of 24-well plates) were collected and washed in ice-cold PBS 24 h after transfection and lysed in ice-cold KHM buffer (110 mM potassium acetate, 20 mM HEPES pH 7.4, 2 mM $MgCl_2$, 0.1 mM digitonin) containing cOmplete™, Mini, EDTA-free protease inhibitor cocktail (Roche). Efficient lysis with KHM buffer required an initial trituration by pipetting and intermittent vortexing over a 10 min incubation on ice. Lysates were centrifuged for 5 min at 3000 rpm in a microfuge at 4°C to pellet insoluble material, and supernatants were then collected on ice and diluted to 0.5 µg/µl in cold KHM buffer after protein concentrations had been determined using the Pierce BCA assay (Thermo Fisher Scientific). The NAD/NADH-Glo™ and NADP/NADPH-Glo™ assays (Promega) were used to measure NAD^+ and $NADP^+$ in extracts. First, 25 µl of each extract was mixed with 12.5 µl 0.4M HCl and heated to 60°C for 15 min to degrade NADH and NADPH before being allowed to cool to room temperature (RT) for 10 min. Reactions were then neutralised by adding 12.5 µl 0.5 M Tris base and 10 µl of each neutralised reaction was mixed with 10 µl of the relevant detection reagent on ice in wells of a 384-well white polystyrene microplate (Corning). Once all reactions had been set up the plate was moved to a GloMax® Explorer plate reader (Promega) and incubated for 40 min at 25°C before reading for luminescence. The CellTiter-Glo® assay (Promega) was used to measure ATP in extracts. Here, 10 µl of extract was mixed

directly with 10 µl of assay reagent on ice in wells of a 384-well white polystyrene microplate. Luminescence was then read after 10 min at 25°C using a GloMax® Explorer plate reader. Concentrations of nucleotides were determined from standard curves generated from dilution series of the relevant nucleotides and then calculated as proportions of the amount in extracts from cells transfected in parallel with empty vector.

Purification of recombinant SARM1 from HEK 293T cells

Recombinant, C-terminal Flag-tagged SARM1 (WT or variant) was purified from HEK 293T cells by immunoprecipitation. HEK cells in 10 cm and 6 cm dishes and individual wells of a 6 cm dish were respectively transfected with 24 µg, 10 µg and 4 µg of SARM1 expression construct. Media was supplemented with 2 mM NR at the time of transfection. Cells were lysed in KHM buffer as for the measurements of nucleotide levels in transfected HEK 293T cells (see above) but extracts were instead diluted to 1 µg/µl in cold KHM buffer after determining protein concentration. For the immunoprecipitation, extracts were incubated overnight at 4°C with rotation with 20 µg/ml anti-FLAG M2 antibody (Merck, F3165) and 50 µl/ml of pre-washed Pierce magnetic protein A/G beads (Thermo Fisher Scientific). Beads were collected on a magnetic rack and washed 3x with KHM buffer and 1x with PBS (with protease inhibitors) and then resuspended in PBS containing 1 mg/ml BSA. Beads were resuspended in 25-50 µl (for low yield proteins and 150 µl (for normal yield proteins) per ml of the immunoprecipitation volume. Inclusion of BSA in the re-suspension buffer allowed samples to be frozen without substantial loss of SARM1 activity (activity is completely lost after one freeze/thaw cycle without its inclusion). The concentrations of SARM1 proteins in the bead suspension were determined by comparison to a standard curve generated from a dilution series of recombinant SARM1 of known concentration (purified from insect cells) after detection by immunoblotting using a rabbit polyclonal antibody raised against human SAM-TIR protein (both kindly provided by AstraZeneca).

Of particular note, the use of KHM lysis buffer is critical for subsequent assaying of the NADase activity of the purified SARM1 protein. Harsher lysis buffers with high concentrations

of strong detergents (e.g., RIPA-based buffers) themselves cause substantial activation of SARM1 NADase a loss of responsiveness to NMN.

NADase assays of recombinant purified SARM1

A series of test assays were first performed to define appropriate concentrations of immunoprecipitated SARM1 proteins and the earliest, reliable assay timepoints to obtain rates as close as possible to the maximal rate under the various reaction conditions used. Optimised reaction conditions were as follows: 25 µl reactions (overall 1x PBS) contained 1 ng/µl SARM1 protein of strong GoF variants (L223P, Δ226-232, Δ249-252, V331E, E340K and T385A) or SAM-TIR, or 5 ng/µl of WT SARM1 and other variants, together with 25 µM NAD^+ ± 10 µM or 50 µM NMN. Reactions were kept on ice until all had been set up. All reactions were performed with the recombinant SARM1 still attached to beads as inefficient elution severely restricted the yield of the poorly-expressed GoF variants. Bead suspensions were thoroughly mixed prior to addition to the reactions. Constitutive (basal) NAD^+ consumption was measured from reactions containing just NAD^+ as the difference between starting levels and levels remaining after a 1 h (for strong GoF variants) or 2 h (for all other variants) incubation at 25°C. NAD^+ consumption in the presence of NMN (both 10 µM and 50 µM) was calculated after a 1 h incubation for all variants. Reactions were each mixed once mid-way through the incubation period to resuspend the beads. To measure NAD^+ using the NAD/NADH-Glo™ assay, 5 µl aliquots of the reaction were removed immediately after setting up (whilst still on ice), to obtain precise starting levels in individual reactions, and after the defined times listed above. Aliquots were then mixed with 2.5 µl of 0.4 M HCl, to stop the reaction, and neutralised by mixing with 2.5 µl 0.5 M Tris base. To bring NAD^+ concentrations down to the linear range of the NAD/NADH-Glo™assay, neutralised samples were subsequently diluted 1 in 50 in a 50% PBS, 25% 0.4 M HCL, 25% 0.5 M Tris base solution, and 10 µl of diluted sample was mixed with 10 µl of detection reagent on ice in wells of a 384-well white polystyrene microplate (Corning). Once all reactions had been set up the plate was moved to a GloMax® Explorer

plate reader (Promega) and incubated for 40 min at 25°C before reading for luminescence. NAD^+ concentrations were determined from standard curves (as above). NAD^+ consumption rates were converted to mol consumed per min per mol of SARM1 protein (mol/min/mol SARM1) to allow direct comparisons. Individual data points for each separate protein preparation are the means of two technical replicates in most cases. Non-specific activity on bead/antibody complexes in control immunoprecipitations (from HEK cells transfected with empty vector) was negligible at less than 0.5% of the NAD^+ consumption of WT or variant SARM1 in assays of basal activity (average of n=4 assays).

Immunoblotting

Extracts from transfected HEK cells used for nucleotide measurements (0.5 µg protein / µl, see above) were diluted 1:2 in 2x SDS-PAGE loading buffer, and bead suspensions of immunoprecipitated recombinant SARM1 proteins were diluted 1:16 for immunoblotting. Samples were incubated at 100°C for 3 mins and 10 µl of sample per lane resolved on 4-20% gradient gels (Bio-Rad) before being transferred to Immobilon-P membrane (Millipore). Blots were blocked in TBS (20 mM Tris p.H. 8.3, 150 mM NaCl) containing 5% skim milk powder for 30 mins at RT before being incubated overnight at 4°C with primary antibody in TBS containing 0.05% Tween-20 (Merck) (TBST) and 5% milk. After 3x 10 min washes in TBST, blots were incubated for 1-2 h at RT with appropriate HRP-conjugated secondary antibodies (diluted 1:3,000, Bio-Rad) in TBST with 5% milk. After 3x 10 min washes in TBST and one rinse in TBS, blots were incubated with Pierce™ ECL Western Blotting Substrate or SuperSignal™ West Dura Extended Duration Substrate (both Thermo Fisher Scientific) and imaged using an Alliance chemiluminescence imaging system (UVITEC Cambridge). Relative band intensities on captured digital images were determined from areas under histogram peaks using Fiji software (http:fiji.sc).

The following primary antibodies were used: mouse monoclonal anti-FLAG M2 (1:2,000, Sigma-Aldrich F3165), mouse monoclonal anti-ZsGreen, clone OTI2C2 (1:1,000, OriGene

Technologies), mouse monoclonal anti-GAPDH, clone 6C5 (1:2,000, Abcam ab8245), mouse anti-β-actin (1:2,000, Merck A5316), mouse monoclonal anti-HA clone 12CA5 (0.1-0.8 µg/ml, Merck) and a rabbit polyclonal antibody raised against human SAM-TIR protein (1:2,000, kindly provided by AstraZeneca). Any adjustment to brightness for presentation in figures was applied to the whole blot.

Primary SCG neuron cultures and microinjection

SCG neuron cultures were prepared from wild-type or *Sarm1*$^{-/-}$ P1-P3 pups and microinjected following established protocols (Gilley & Loreto, 2020). Mice were used in accordance with the Home Office Animal Scientific Procedures Act (ASPA), 1986 under project licence P98A03BF9. Dissected SCG ganglia were incubated at 37°C for 20 min in 0.025% trypsin (Sigma) dissolved in PBS followed by 20 min in 0.2% collagenase type II (Gibco) in PBS (with calcium and magnesium). After, ganglia were gently triturated using a pipette tip in SCG culture medium comprising Dulbecco's Modified Eagle's Medium (DMEM) (4500 mg/L glucose and 110 mg/L sodium pyruvate, Sigma) supplemented with 2 mM glutamine (Invitrogen), 1% penicillin/streptomycin (Invitrogen), 10% fetal bovine serum (Sigma), 2 µg/ml aphidicolin (Calbiochem), and 100 ng/ml 7S NGF (Invitrogen). After a 1-2 h pre-plating stage to remove non-neuronal cells, dissociated neurons were plated in a small laminin-coated area on ibidi µ-dishes pre-coated with poly-L-lysine (Thistle Scientific). Cultures were maintained in SCG medium, which was changed every 2-3 days, and were injected after 5-7 days. The inclusion of aphidicolin in the medium suppressed growth and proliferation of any non-neuronal cells.

SCG neurons were microinjected using a Zeiss Axiovert 200 microscope with an Eppendorf 5171 transjector and 5246 micromanipulator system and Eppendorf Femtotips. Expression constructs were diluted in 0.5x PBS and cleared by spinning through a Spin-X filter (Costar). The mix was injected into the nuclei of SCG neurons. The concentrations of expression constructs in the injection mix are listed in Figure legends. 45 neurons were injected per dish. Although ZsGreen is co-expressed from the SARM1 vector used in these studies, restricting the amount of vector injected to limit SARM1 expression meant that the

resulting ZsGreen expression was itself not sufficient for clear visualisation of injected neurons and their neurites. For the purposes of visualisation we thus had to co-inject a DsRed expression construct at a higher concentration.

Imaging

Fluorescence and phase contrast images of transfected HEK 293T cells and injected SCG neurons were acquired with a Leica DFC365FX fluorescence monochrome camera attached to a Leica DMi8 inverted fluorescence microscope using 10x and 20x objectives.

ALS patient details and database resources

This is a retrospective study using anonymised data so specific consent was not obtained by the authors, but consent was obtained at each site that contributed patient information to this study in accordance with their local Institutional Review Boards (IRBs). Patient information for the Answer ALS project patients (patient IDs NEUMA411HJP and NEUBD218YR3) was already publicly available at https://dataportal.answerals.org/search. Information for *SARM1* variants in the Answer ALS project was obtained using ANNOVAR (Wang et al., 2010) annotation on Genome Reference Consortium Human Build 38 (hg38) positions, after read mapping with Burrows-Wheeler Alignment tool (BWA) (Li & Durbin, 2010), variant calling with GATK (20644199), and joint-genotype using Sentieon (Freed et al., 2017). The Project MinE initiative data browser for Data Freeze 1 for searching genetic variation in patient and control cohorts can be accessed at http://databrowser.projectmine.com/. Non-public patient and sequencing datasets and additional clinical information for specific patients can be obtained on request from the corresponding author.

Statistics

Unmatched or repeated measures (for matched/paired data) multiple comparisons were performed (using one- or two-way ANOVA or multiple *t* tests) with a false discovery rate (FDR) correction (original Benjamini and Hochberg method) using Prism software (GraphPad

Software Inc., La Jolla, CA, USA). Log transformation of the data was performed if they did not initially meet the assumptions for a parametric test, namely normality and homogeneity of variance, as appropriate (Figures 2A, 2C, 3A, 4A-C and 6A and Supplementary Figure 4). A *p* value of >0.05 was considered not significant (n.s.) and **p*<0.05, ***p*<0.01, and ****p*<0.001. To determine whether there is a burden of rare variants (minor allele frequency <0.01) in the *SARM*1 gene and its domains, we performed burden and optimized sequence kernel association test (SKAT-O) as implemented in the SKAT-O R package (Lee et al., 2012). The tests were done first at the gene level, followed by domain-by-domain analysis, corrected for false discovery rate. Since we identified a burden of rare variants in the ARM domain driven by GoF variants (see Results), we examined additional datasets in which we further tested the burden of rare GoF variants. A χ^2 test (with Yates' correction) was used to test enrichment of the single Δ226-232 *SARM1* variant in ALS/HSP patients.

ACKNOWLEDGMENTS

This work was supported by a grant from the Robert Packard Center for ALS Research at Johns Hopkins and was supported in part by data provided by the Answer ALS Consortium – also administered by the Robert Packard Center. Its contents are solely the responsibility of the authors and do not necessarily represent the official views of The Johns Hopkins University or any grantor proving funds to its Robert Packard Center for ALS Research. Additional support was provided by a BBSRC/AstraZeneca Industrial Partnership Award BB/S009582/1 (for functional characterisation of SARM1) and Wellcome Trust Collaborative Award 220906/Z/20/Z. Anne Segonds-Pichon kindly helped with statistical analyses. We are grateful to the following for accessing Project MinE data: Evelijn Zeijdner, Jan Veldink, Kristel van Eijk (all UMC Utrecht) and Alfredo Iacoangeli (Institute of Psychiatry, King's College London). We also thank the following for useful discussion and feedback: Jemeen Sreedharan, Ammar Al-Chalabi, Ahmet Höke, David Bennett, Steve Finkbeiner, Henry Houlden, Jonathan Cooper-Knock, Giuseppe Orsomando and all members of the Coleman group.

COMPETING INTERESTS

Funding of academic projects from AstraZeneca and M.P.C. is a consultant for Nura Bio.

AUTHOR CONTRIBUTIONS

J.G. and M.P.C. conceived the study. J.G. designed and performed all experiments with help from O.J. M.P., Q.S.G. and M.M.R provided intellectual input into project development and information relating to the UCL cohort patient. M.A.E, Z.G-O., S.A.G., M.B.H., J.K., L.L., J.R., G.A.R, and S.Z. each provided clinical details of specific patients and/or cohort analysis. J.G. and M.P.C. wrote the manuscript with input from all other authors. All authors read and approved the manuscript.

REFERENCES

Arai, T., Hasegawa, M., Akiyama, H., Ikeda, K., Nonaka, T., Mori, H., Mann, D., Tsuchiya, K., Yoshida, M., Hashizume, Y., & Oda, T. (2006). TDP-43 is a component of ubiquitin-positive tau-negative inclusions in frontotemporal lobar degeneration and amyotrophic lateral sclerosis. *Biochemical and Biophysical Research Communications*, *351*(3), 602–611. https://doi.org/10.1016/j.bbrc.2006.10.093

Bloom, A. J., Mao, X., Strickland, A., Sasaki, Y., Milbrandt, J., & DiAntonio, A. (2021). Constitutively active SARM1 variants found in ALS patients induce neuropathy. *BioRxiv*, 2021.04.16.439886. https://doi.org/10.1101/2021.04.16.439886

Bosanac, T., Hughes, R. O., Engber, T., Devraj, R., Brearley, A., Danker, K., Young, K., Kopatz, J., Hermann, M., Berthemy, A., Boyce, S., Bentley, J., & Krauss, R. (2021). Pharmacological SARM1 inhibition protects axon structure and function in paclitaxel-induced peripheral neuropathy. *Brain: A Journal of Neurology*. https://doi.org/10.1093/brain/awab184

Bratkowski, M., Xie, T., Thayer, D. A., Lad, S., Mathur, P., Yang, Y.-S., Danko, G., Burdett, T. C., Danao, J., Cantor, A., Kozak, J. A., Brown, S. P., Bai, X., & Sambashivan, S. (2020). Structural and Mechanistic Regulation of the Pro-degenerative NAD Hydrolase SARM1. *Cell Reports*, *32*(5), 107999. https://doi.org/10.1016/j.celrep.2020.107999

Coleman, M. P., & Höke, A. (2020). Programmed axon degeneration: From mouse to mechanism to medicine. *Nature Reviews. Neuroscience*, *21*(4), 183–196. https://doi.org/10.1038/s41583-020-0269-3

Conforti, L., Gilley, J., & Coleman, M. P. (2014). Wallerian degeneration: An emerging axon death pathway linking injury and disease. *Nature Reviews. Neuroscience*, *15*(6), 394–409. https://doi.org/10.1038/nrn3680

Di Stefano, M., Nascimento-Ferreira, I., Orsomando, G., Mori, V., Gilley, J., Brown, R., Janeckova, L., Vargas, M. E., Worrell, L. A., Loreto, A., Tickle, J., Patrick, J., Webster, J. R. M., Marangoni, M., Carpi, F. M., Pucciarelli, S., Rossi, F., Meng, W., Sagasti, A., … Conforti, L. (2015). A rise in NAD precursor nicotinamide mononucleotide (NMN) after injury promotes axon degeneration. *Cell Death and Differentiation*, *22*(5), 731–742. https://doi.org/10.1038/cdd.2014.164

Di Stefano, Michele, Loreto, A., Orsomando, G., Mori, V., Zamporlini, F., Hulse, R. P., Webster, J., Donaldson, L. F., Gering, M., Raffaelli, N., Coleman, M. P., Gilley, J., & Conforti, L. (2017). NMN Deamidase Delays Wallerian Degeneration and Rescues Axonal Defects Caused by NMNAT2 Deficiency In Vivo. *Current Biology: CB*, *27*(6), 784–794. https://doi.org/10.1016/j.cub.2017.01.070

Essuman, K., Summers, D. W., Sasaki, Y., Mao, X., DiAntonio, A., & Milbrandt, J. (2017). The SARM1 Toll/Interleukin-1 Receptor Domain Possesses Intrinsic NAD+ Cleavage Activity that Promotes Pathological Axonal Degeneration. *Neuron*, *93*(6), 1334-1343.e5. https://doi.org/10.1016/j.neuron.2017.02.022

Essuman, K., Summers, D. W., Sasaki, Y., Mao, X., Yim, A. K. Y., DiAntonio, A., & Milbrandt, J. (2018). TIR Domain Proteins Are an Ancient Family of NAD+-Consuming Enzymes. *Current Biology*, *28*(3), 421-430.e4. https://doi.org/10.1016/j.cub.2017.12.024

Figley, M. D., & DiAntonio, A. (2020). The SARM1 axon degeneration pathway: Control of the NAD+ metabolome regulates axon survival in health and disease. *Current Opinion in Neurobiology*, *63*, 59–66. https://doi.org/10.1016/j.conb.2020.02.012

Figley, M. D., Gu, W., Nanson, J. D., Shi, Y., Sasaki, Y., Cunnea, K., Malde, A. K., Jia, X., Luo, Z., Saikot, F. K., Mosaiab, T., Masic, V., Holt, S., Hartley-Tassell, L., McGuinness, H. Y., Manik, M. K., Bosanac, T., Landsberg, M. J., Kerry, P. S., … Ve, T. (2021). SARM1 is

a metabolic sensor activated by an increased NMN/NAD+ ratio to trigger axon degeneration. *Neuron*, *109*(7), 1118-1136.e11. https://doi.org/10.1016/j.neuron.2021.02.009

Fogh, I., Ratti, A., Gellera, C., Lin, K., Tiloca, C., Moskvina, V., Corrado, L., Sorarù, G., Cereda, C., Corti, S., Gentilini, D., Calini, D., Castellotti, B., Mazzini, L., Querin, G., Gagliardi, S., Del Bo, R., Conforti, F. L., Siciliano, G., … SLAGEN Consortium and Collaborators. (2014). A genome-wide association meta-analysis identifies a novel locus at 17q11.2 associated with sporadic amyotrophic lateral sclerosis. *Human Molecular Genetics*, *23*(8), 2220–2231. https://doi.org/10.1093/hmg/ddt587

Freed, D., Aldana, R., Weber, J. A., & Edwards, J. S. (2017). The Sentieon Genomics Tools—A fast and accurate solution to variant calling from next-generation sequence data. *BioRxiv*, 115717. https://doi.org/10.1101/115717

Geisler, S., Huang, S. X., Strickland, A., Doan, R. A., Summers, D. W., Mao, X., Park, J., DiAntonio, A., & Milbrandt, J. (2019). Gene therapy targeting SARM1 blocks pathological axon degeneration in mice. *The Journal of Experimental Medicine*, *216*(2), 294–303. https://doi.org/10.1084/jem.20181040

Gerdts, J., Brace, E. J., Sasaki, Y., DiAntonio, A., & Milbrandt, J. (2015). SARM1 activation triggers axon degeneration locally via NAD^+ destruction. *Science (New York, N.Y.)*, *348*(6233), 453–457. https://doi.org/10.1126/science.1258366

Gerdts, J., Summers, D. W., Milbrandt, J., & DiAntonio, A. (2016). Axon Self-Destruction: New Links among SARM1, MAPKs, and NAD+ Metabolism. *Neuron*, *89*(3), 449–460. https://doi.org/10.1016/j.neuron.2015.12.023

Gerdts, J., Summers, D. W., Sasaki, Y., DiAntonio, A., & Milbrandt, J. (2013). Sarm1-mediated axon degeneration requires both SAM and TIR interactions. *The Journal of Neuroscience: The Official Journal of the Society for Neuroscience*, *33*(33), 13569–13580. https://doi.org/10.1523/JNEUROSCI.1197-13.2013

Gilley, J., Adalbert, R., Yu, G., & Coleman, M. P. (2013). Rescue of peripheral and CNS axon defects in mice lacking NMNAT2. *The Journal of Neuroscience: The Official Journal of the Society for Neuroscience*, *33*(33), 13410–13424. https://doi.org/10.1523/JNEUROSCI.1534-13.2013

Gilley, J., & Coleman, M. P. (2010). Endogenous Nmnat2 is an essential survival factor for maintenance of healthy axons. *PLoS Biology*, *8*(1), e1000300. https://doi.org/10.1371/journal.pbio.1000300

Gilley, J., & Loreto, A. (2020). Microinjection of Superior Cervical Ganglion Neurons for Studying Axon Degeneration. *Methods in Molecular Biology (Clifton, N.J.)*, *2143*, 25–39. https://doi.org/10.1007/978-1-0716-0585-1_3

Gilley, J., Mayer, P. R., Yu, G., & Coleman, M. P. (2019). Low levels of NMNAT2 compromise axon development and survival. *Human Molecular Genetics*, *28*(3), 448–458. https://doi.org/10.1093/hmg/ddy356

Gilley, J., Orsomando, G., Nascimento-Ferreira, I., & Coleman, M. P. (2015). Absence of SARM1 rescues development and survival of NMNAT2-deficient axons. *Cell Reports*, *10*(12), 1974–1981. https://doi.org/10.1016/j.celrep.2015.02.060

Gonzalez, M., Falk, M. J., Gai, X., Postrel, R., Schüle, R., & Zuchner, S. (2015). Innovative genomic collaboration using the GENESIS (GEM.app) platform. *Human Mutation*, *36*(10), 950–956. https://doi.org/10.1002/humu.22836

Goutman, S. A. (2017). Diagnosis and Clinical Management of Amyotrophic Lateral Sclerosis and Other Motor Neuron Disorders. *Continuum (Minneapolis, Minn.)*, *23*(5, Peripheral Nerve and Motor Neuron Disorders), 1332–1359. https://doi.org/10.1212/CON.0000000000000535

Horsefield, S., Burdett, H., Zhang, X., Manik, M. K., Shi, Y., Chen, J., Qi, T., Gilley, J., Lai, J.-S., Rank, M. X., Casey, L. W., Gu, W., Ericsson, D. J., Foley, G., Hughes, R. O., Bosanac, T., von Itzstein, M., Rathjen, J. P., Nanson, J. D., … Kobe, B. (2019). NAD+ cleavage activity by animal and plant TIR domains in cell death pathways. *Science (New York, N.Y.)*, *365*(6455), 793–799. https://doi.org/10.1126/science.aax1911

Hughes, R. O., Bosanac, T., Mao, X., Engber, T. M., DiAntonio, A., Milbrandt, J., Devraj, R., & Krauss, R. (2021). Small Molecule SARM1 Inhibitors Recapitulate the SARM1-/- Phenotype and Allow Recovery of a Metastable Pool of Axons Fated to Degenerate. *Cell Reports*, *34*(1), 108588. https://doi.org/10.1016/j.celrep.2020.108588

Huppke, P., Wegener, E., Gilley, J., Angeletti, C., Kurth, I., Drenth, J. P. H., Stadelmann, C., Barrantes-Freer, A., Brück, W., Thiele, H., Nürnberg, P., Gärtner, J., Orsomando, G., & Coleman, M. P. (2019). Homozygous NMNAT2 mutation in sisters with polyneuropathy and erythromelalgia. *Experimental Neurology*, *320*, 112958. https://doi.org/10.1016/j.expneurol.2019.112958

Jiang, Y., Liu, T., Lee, C.-H., Chang, Q., Yang, J., & Zhang, Z. (2020). The NAD+-mediated self-inhibition mechanism of pro-neurodegenerative SARM1. *Nature*, *588*(7839), 658–663. https://doi.org/10.1038/s41586-020-2862-z

Klim, J. R., Williams, L. A., Limone, F., Guerra San Juan, I., Davis-Dusenbery, B. N., Mordes, D. A., Burberry, A., Steinbaugh, M. J., Gamage, K. K., Kirchner, R., Moccia, R., Cassel, S. H., Chen, K., Wainger, B. J., Woolf, C. J., & Eggan, K. (2019). ALS-implicated protein TDP-43 sustains levels of STMN2, a mediator of motor neuron growth and repair. *Nature Neuroscience*, *22*(2), 167–179. https://doi.org/10.1038/s41593-018-0300-4

Lee, J., Shin, M.-K., Ryu, D.-K., Kim, S., & Ryu, W.-S. (2010). Insertion and deletion mutagenesis by overlap extension PCR. *Methods in Molecular Biology (Clifton, N.J.)*, *634*, 137–146. https://doi.org/10.1007/978-1-60761-652-8_10

Lee, S., Emond, M. J., Bamshad, M. J., Barnes, K. C., Rieder, M. J., Nickerson, D. A., NHLBI GO Exome Sequencing Project—ESP Lung Project Team, Christiani, D. C., Wurfel, M. M., & Lin, X. (2012). Optimal unified approach for rare-variant association testing with application to small-sample case-control whole-exome sequencing studies. *American Journal of Human Genetics*, *91*(2), 224–237. https://doi.org/10.1016/j.ajhg.2012.06.007

Li, H., & Durbin, R. (2010). Fast and accurate long-read alignment with Burrows-Wheeler transform. *Bioinformatics (Oxford, England)*, *26*(5), 589–595. https://doi.org/10.1093/bioinformatics/btp698

Lopate, G., Baloh, R. H., Al-Lozi, M. T., Miller, T. M., Filho, J. A. F., Ni, O., Leston, A., Florence, J., Schierbecker, J., & Allred, P. (2010). Familial ALS with extreme phenotypic variability due to the I113T SOD1 mutation. *Amyotrophic Lateral Sclerosis*, *11*(1–2), 232–236. https://doi.org/10.3109/17482960902898069

Loreto, A., Angeletti, C., Gilley, J., Arthur-Farraj, P., Merlini, E., Amici, A., Desrochers, L. M., Wang, Q., Orsomando, G., & Coleman, M. P. (2020). Potent activation of SARM1 by NMN analogue VMN underlies vacor neurotoxicity. *BioRxiv*, 2020.09.18.304261. https://doi.org/10.1101/2020.09.18.304261

Lukacs, M., Gilley, J., Zhu, Y., Orsomando, G., Angeletti, C., Liu, J., Yang, X., Park, J., Hopkin, R. J., Coleman, M. P., Zhai, R. G., & Stottmann, R. W. (2019). Severe biallelic loss-of-function mutations in nicotinamide mononucleotide adenylyltransferase 2 (NMNAT2) in two fetuses with fetal akinesia deformation sequence. *Experimental Neurology*, *320*, 112961. https://doi.org/10.1016/j.expneurol.2019.112961

Mackenzie, I. R. A., Bigio, E. H., Ince, P. G., Geser, F., Neumann, M., Cairns, N. J., Kwong, L. K., Forman, M. S., Ravits, J., Stewart, H., Eisen, A., McClusky, L., Kretzschmar, H. A.,

Monoranu, C. M., Highley, J. R., Kirby, J., Siddique, T., Shaw, P. J., Lee, V. M.-Y., & Trojanowski, J. Q. (2007). Pathological TDP-43 distinguishes sporadic amyotrophic lateral sclerosis from amyotrophic lateral sclerosis with SOD1 mutations. *Annals of Neurology*, *61*(5), 427–434. https://doi.org/10.1002/ana.21147

Maekawa, S., Leigh, P. N., King, A., Jones, E., Steele, J. C., Bodi, I., Shaw, C. E., Hortobagyi, T., & Al-Sarraj, S. (2009). TDP-43 is consistently co-localized with ubiquitinated inclusions in sporadic and Guam amyotrophic lateral sclerosis but not in familial amyotrophic lateral sclerosis with and without SOD1 mutations. *Neuropathology: Official Journal of the Japanese Society of Neuropathology*, *29*(6), 672–683. https://doi.org/10.1111/j.1440-1789.2009.01029.x

McAlary, L., Plotkin, S. S., Yerbury, J. J., & Cashman, N. R. (2019). Prion-Like Propagation of Protein Misfolding and Aggregation in Amyotrophic Lateral Sclerosis. *Frontiers in Molecular Neuroscience*, *12*. https://doi.org/10.3389/fnmol.2019.00262

Melamed, Z., López-Erauskin, J., Baughn, M. W., Zhang, O., Drenner, K., Sun, Y., Freyermuth, F., McMahon, M. A., Beccari, M. S., Artates, J. W., Ohkubo, T., Rodriguez, M., Lin, N., Wu, D., Bennett, C. F., Rigo, F., Da Cruz, S., Ravits, J., Lagier-Tourenne, C., & Cleveland, D. W. (2019). Premature polyadenylation-mediated loss of stathmin-2 is a hallmark of TDP-43-dependent neurodegeneration. *Nature Neuroscience*, *22*(2), 180–190. https://doi.org/10.1038/s41593-018-0293-z

Neumann, M., Sampathu, D. M., Kwong, L. K., Truax, A. C., Micsenyi, M. C., Chou, T. T., Bruce, J., Schuck, T., Grossman, M., Clark, C. M., McCluskey, L. F., Miller, B. L., Masliah, E., Mackenzie, I. R., Feldman, H., Feiden, W., Kretzschmar, H. A., Trojanowski, J. Q., & Lee, V. M.-Y. (2006). Ubiquitinated TDP-43 in frontotemporal lobar degeneration and amyotrophic lateral sclerosis. *Science (New York, N.Y.)*, *314*(5796), 130–133. https://doi.org/10.1126/science.1134108

Nicholson, G., Lenk, G. M., Reddel, S. W., Grant, A. E., Towne, C. F., Ferguson, C. J., Simpson, E., Scheuerle, A., Yasick, M., Hoffman, S., Blouin, R., Brandt, C., Coppola, G., Biesecker, L. G., Batish, S. D., & Meisler, M. H. (2011). Distinctive genetic and clinical features of CMT4J: A severe neuropathy caused by mutations in the PI(3,5)P_2 phosphatase FIG4. *Brain: A Journal of Neurology*, *134*(Pt 7), 1959–1971. https://doi.org/10.1093/brain/awr148

Osterloh, J. M., Yang, J., Rooney, T. M., Fox, A. N., Adalbert, R., Powell, E. H., Sheehan, A. E., Avery, M. A., Hackett, R., Logan, M. A., MacDonald, J. M., Ziegenfuss, J. S., Milde, S., Hou, Y.-J., Nathan, C., Ding, A., Brown, R. H., Conforti, L., Coleman, M., … Freeman, M. R. (2012). DSarm/Sarm1 is required for activation of an injury-induced axon death pathway. *Science (New York, N.Y.)*, *337*(6093), 481–484. https://doi.org/10.1126/science.1223899

Ozaki, E., Gibbons, L., Neto, N. G., Kenna, P., Carty, M., Humphries, M., Humphries, P., Campbell, M., Monaghan, M., Bowie, A., & Doyle, S. L. (2020). SARM1 deficiency promotes rod and cone photoreceptor cell survival in a model of retinal degeneration. *Life Science Alliance*, *3*(5). https://doi.org/10.26508/lsa.201900618

Panneerselvam, P., Singh, L. P., Ho, B., Chen, J., & Ding, J. L. (2012). Targeting of pro-apoptotic TLR adaptor SARM to mitochondria: Definition of the critical region and residues in the signal sequence. *The Biochemical Journal*, *442*(2), 263–271. https://doi.org/10.1042/BJ20111653

Peters, O. M., Lewis, E. A., Osterloh, J. M., Weiss, A., Salameh, J. S., Metterville, J., Brown, R. H., & Freeman, M. R. (2018). Loss of Sarm1 does not suppress motor neuron degeneration in the SOD1G93A mouse model of amyotrophic lateral sclerosis. *Human Molecular Genetics*, *27*(21), 3761–3771. https://doi.org/10.1093/hmg/ddy260

Project MinE ALS Sequencing Consortium. (2018). Project MinE: Study design and pilot analyses of a large-scale whole-genome sequencing study in amyotrophic lateral sclerosis. *European Journal of Human Genetics: EJHG*, *26*(10), 1537–1546. https://doi.org/10.1038/s41431-018-0177-4

Rossor, A. M., Kalmar, B., Greensmith, L., & Reilly, M. M. (2012). The distal hereditary motor neuropathies. *Journal of Neurology, Neurosurgery, and Psychiatry*, *83*(1), 6–14. https://doi.org/10.1136/jnnp-2011-300952

Rothstein, J. (2020, October 28). *Answer ALS: A Large-Scale Resource for Sporadic and Familial ALS Combining Clinical Data with Multi-Omics Data from Induced Pluripotent Cell Lines*. https://doi.org/10.21203/rs.3.rs-96858/v1

Sasaki, Y., Kakita, H., Kubota, S., Sene, A., Lee, T. J., Ban, N., Dong, Z., Lin, J. B., Boye, S. L., DiAntonio, A., Boye, S. E., Apte, R. S., & Milbrandt, J. (2020). SARM1 depletion rescues NMNAT1-dependent photoreceptor cell death and retinal degeneration. *ELife*, *9*. https://doi.org/10.7554/eLife.62027

Shen, C., Vohra, M., Zhang, P., Mao, X., Figley, M. D., Zhu, J., Sasaki, Y., Wu, H., DiAntonio, A., & Milbrandt, J. (2021). Multiple domain interfaces mediate SARM1 autoinhibition. *Proceedings of the National Academy of Sciences of the United States of America*, *118*(4). https://doi.org/10.1073/pnas.2023151118

Shin, J. E., Miller, B. R., Babetto, E., Cho, Y., Sasaki, Y., Qayum, S., Russler, E. V., Cavalli, V., Milbrandt, J., & DiAntonio, A. (2012). SCG10 is a JNK target in the axonal degeneration pathway. *Proceedings of the National Academy of Sciences of the United States of America*, *109*(52), E3696-3705. https://doi.org/10.1073/pnas.1216204109

Sporny, M., Guez-Haddad, J., Khazma, T., Yaron, A., Dessau, M., Shkolnisky, Y., Mim, C., Isupov, M. N., Zalk, R., Hons, M., & Opatowsky, Y. (2020). Structural basis for SARM1 inhibition and activation under energetic stress. *ELife*, *9*. https://doi.org/10.7554/eLife.62021

Sporny, M., Guez-Haddad, J., Lebendiker, M., Ulisse, V., Volf, A., Mim, C., Isupov, M. N., & Opatowsky, Y. (2019). Structural Evidence for an Octameric Ring Arrangement of SARM1. *Journal of Molecular Biology*, *431*(19), 3591–3605. https://doi.org/10.1016/j.jmb.2019.06.030

Summers, D. W., DiAntonio, A., & Milbrandt, J. (2014). Mitochondrial dysfunction induces Sarm1-dependent cell death in sensory neurons. *The Journal of Neuroscience: The Official Journal of the Society for Neuroscience*, *34*(28), 9338–9350. https://doi.org/10.1523/JNEUROSCI.0877-14.2014

Summers, D. W., Gibson, D. A., DiAntonio, A., & Milbrandt, J. (2016). SARM1-specific motifs in the TIR domain enable NAD+ loss and regulate injury-induced SARM1 activation. *Proceedings of the National Academy of Sciences of the United States of America*, *113*(41), E6271–E6280. https://doi.org/10.1073/pnas.1601506113

Theunissen, F., Anderton, R. S., Mastaglia, F. L., Flynn, L. L., Winter, S. J., James, I., Bedlack, R., Hodgetts, S., Fletcher, S., Wilton, S. D., Laing, N. G., MacShane, M., Needham, M., Saunders, A., Mackay-Sim, A., Melamed, Z., Ravits, J., Cleveland, D. W., & Akkari, P. A. (2021). Novel STMN2 Variant Linked to Amyotrophic Lateral Sclerosis Risk and Clinical Phenotype. *Frontiers in Aging Neuroscience*, *13*, 658226. https://doi.org/10.3389/fnagi.2021.658226

van Rheenen, W., Shatunov, A., Dekker, A. M., McLaughlin, R. L., Diekstra, F. P., Pulit, S. L., van der Spek, R. A. A., Võsa, U., de Jong, S., Robinson, M. R., Yang, J., Fogh, I., van Doormaal, P. T., Tazelaar, G. H. P., Koppers, M., Blokhuis, A. M., Sproviero, W., Jones, A. R., Kenna, K. P., … Veldink, J. H. (2016). Genome-wide association analyses identify

new risk variants and the genetic architecture of amyotrophic lateral sclerosis. *Nature Genetics*, *48*(9), 1043–1048. https://doi.org/10.1038/ng.3622

Wan, L., Essuman, K., Anderson, R. G., Sasaki, Y., Monteiro, F., Chung, E.-H., Osborne Nishimura, E., DiAntonio, A., Milbrandt, J., Dangl, J. L., & Nishimura, M. T. (2019). TIR domains of plant immune receptors are NAD+-cleaving enzymes that promote cell death. *Science (New York, N.Y.)*, *365*(6455), 799–803. https://doi.org/10.1126/science.aax1771

Wang, K., Li, M., & Hakonarson, H. (2010). ANNOVAR: Functional annotation of genetic variants from high-throughput sequencing data. *Nucleic Acids Research*, *38*(16), e164. https://doi.org/10.1093/nar/gkq603

White, M. A., Lin, Z., Kim, E., Henstridge, C. M., Pena Altamira, E., Hunt, C. K., Burchill, E., Callaghan, I., Loreto, A., Brown-Wright, H., Mead, R., Simmons, C., Cash, D., Coleman, M. P., & Sreedharan, J. (2019). Sarm1 deletion suppresses TDP-43-linked motor neuron degeneration and cortical spine loss. *Acta Neuropathologica Communications*, *7*(1), 166. https://doi.org/10.1186/s40478-019-0800-9

Zhao, Z. Y., Xie, X. J., Li, W. H., Liu, J., Chen, Z., Zhang, B., Li, T., Li, S. L., Lu, J. G., Zhang, L., Zhang, L.-H., Xu, Z., Lee, H. C., & Zhao, Y. J. (2019). A Cell-Permeant Mimetic of NMN Activates SARM1 to Produce Cyclic ADP-Ribose and Induce Non-apoptotic Cell Death. *IScience*, *15*, 452–466. https://doi.org/10.1016/j.isci.2019.05.001

FIGURE LEGENDS

Figure 1. SARM1 coding variants in Project MinE patient and control groups.

Schematic representation of the canonical 724 amino acid human SARM1 protein showing basic domain structure and the approximate locations of the coding variation present in the 4,366 ALS patients and 1,832 control individuals in the original Project MinE DF1 release. Variants are classified based on which cohort(s) they appear in.

Special note: in Project MinE DF1 (and gnomAD v2.1.1), SARM1 variants are annotated to a 690 amino acid product of a non-canonical reference cDNA sequence containing sequencing errors at the 5' end (single nucleotide substitutions, insertions and deletions) resulting in a truncated N-terminus due to predicted use of an alternative ATG codon and frame switching until the predicted open reading frame eventually synchronises with the canonical 724 amino acid SARM1 at amino acid 107 (73 in the 690 amino acid "isoform"). As such, numbering of SARM1 variants in Project MinE (and gnomAD v2.11) over the synchronised region is 34 residues lower than the correct numbering as shown in the above schematic. Correct annotation is used in the NCBI Single Nucleotide Polymorphism Database (dbSNP, including rsIDs) and gnomAD v3.1.1.

Figure 2. Several ALS patient-specific SARM1 ARM domain coding variants in Project MinE increase NAD^+ depletion in transfected HEK cells.

(A-C) Relative levels of NAD^+ (A), ATP (B) and $NADP^+$ (C) in extracts of HEK 293T cells 24 h after transfection with expression constructs for Flag-tagged WT or variant SARM1 (as listed). 50 ng SARM1 vector was combined with 750 ng empty vector (24-well plate format) to optimise the assay (see Supplementary Figure 1). Data are shown as a proportion of levels in cells transfected with empty vector (ev) alone, performed in parallel. Means ±SEM with individual data points are plotted (n=4 or 5). *p<0.05, **p<0.01 and ***p<0.001, multiple comparisons versus WT SARM1 with FDR correction. WT SARM1, and P332Q and N337D

SARM1 (seen in patient and control groups in Project MinE) are shown as hatched bars to differentiate them from patient-specific variants.

(D) Representative immunoblots of extracts, as described for (A-C), showing Flag-tagged WT or variant SARM1 (~70 kDa), ZsGreen (~26 kDa, co-expressed with the exogenous SARM1 from a bicistronic mRNA) and GAPDH (~36 kDa, acting as a loading control). Four times the amount of extract and enhanced detection was needed to detect strong GoF SARM1 variants (bottom right of panel).

(E) Representative ZsGeen fluorescence and phase contrast imaging of HEK 293T cells 24 h after transfection with WT or Δ226-232 SARM1 expression constructs (brightness and contrast have been increased equally in each pair of images to enhance visualisation of zsGreen-positive cells in the Δ226-232 image). Reduced ZsGreen signal intensity, as seen here for Δ226-232 SARM1, was consistently seen (n=5) for variants that reduced NAD^+ levels more than WT SARM1.

Figure 3. The effects of Δ226-232 SARM1 are dominant when co-expressed with WT SARM1 in HEK cells.

(A) Relative levels of NAD^+ in extracts of HEK 293T cells 24 h after transfection with a mixture of expression constructs for Flag- or HA-tagged WT SARM1 (WT[F] and WT[HA] respectively) and/or Flag-tagged Δ226-232 SARM1 (Δ226-232[F]). A total of 50 ng SARM1 vector (50 ng of a single construct or 25 ng each of two constructs) was mixed with 750 ng empty vector (24-well plate format). NAD^+ levels are shown as a proportion of those in cells transfected with empty vector (ev) alone, performed in parallel. Means ±SEM with individual data points (n=6) are plotted. ***$p<0.001$ and n.s. = $p>0.05$, repeated measures multiple comparisons with FDR correction (only relevant comparisons are shown).

(B) Representative immunoblots of extracts as described in (A). Separate, duplicate blots were probed with Flag or HA antibodies to independently assess levels of Flag- or HA-tagged WT or Δ226-232 SARM1 (~70 kDa). Both blots were also probed with antibodies against ZsGreen (~26 kDa) and GAPDH (~36 kDa, acting as a loading control) to ensure the blots were true

replicates. A faint, non-specific cross-reaction of the HA antibody to Flag-tagged SARM1 was consistently seen (as per WT[F] only lane).

Figure 4. Constitutive (basal) NADase activity and NMN responsiveness of SARM1 ARM domain variants in Project MinE.

(A) Constitutive NADase activities of immunoprecipitated WT or variant SARM1 in the presence of 25 μM NAD^+. Variants with high or low NADase activity are plotted separately, against different scales, to more clearly show all differences relative to WT SARM1 (included on both). Means ±SEM with individual data points (n=4) are plotted. *p<0.05 and ***p<0.001, repeated measures multiple comparisons versus WT SARM1 with FDR correction.

(B) Activation of SARM1 NADase by 50 μm NMN (for 25 μM NAD^+). Basal activities (no NMN) are as in (A) but rates ±NMN were calculated from assays performed in parallel. High and low NADase activity variants are again plotted separately (as in part A). Means ±SEM with individual data points (n=4) are plotted. *p<0.05 and **p<0.01, repeated measures multiple comparisons of rates ±NMN (for each variant) with FDR correction.

(C) Relative activation of SARM1 NADase by 10 or 50 μm NMN (for 25 μM NAD^+). NMN-insensitive variants with very high basal NADase activity were not tested. Basal and +50 μM NMN activities are a subset of those shown in (B) and are those from assays performed in parallel with 10 μM NMN. Means ±SEM with individual data points (n=3) are plotted. *p<0.05 and **p<0.01, repeated measures multiple comparisons of rates ±NMN (for each variant) with FDR correction.

Each panel was designed to show different statistical comparisons and some of the same data was used for multiple tests, as described. WT SARM1, and P332Q and N337D SARM1 (seen in patient and control groups in Project MinE), are shown as hatched bars throughout to differentiate them from patient-specific variants.

Figure 5. Strong GoF Δ226-232 SARM1 reduces SCG neuron viability under mild stress conditions.

(A) Representative images of DsRed-positive (wild-type) SCG neurons, ± 2 mM NR in the culture media, 24 h after microinjection with expression constructs for WT or Δ226-232 SARM1 and DsRed (at 2.5 ng/µl and 40 ng/µl in the injection mix, respectively). Equal numbers of neurons were injected.

(B) Quantification of DsRed-positive neurons for conditions described in (A). Means ±SEM with individual data points (n=5 or 17) are plotted. *p<0.05 and ***p<0.001, multiple comparisons with FDR correction (only relevant comparisons are shown).

(C) Time course of survival of DsRed-positive neurons manipulated as indicated. Neurons were injected as in (A). Manipulations were performed 24 h after injection, corresponding to time 0 on the graphs. Survival of injected neurons was assessed as described in (D). Means ±SEM (n=4) are plotted. ***p<0.001, repeated measures multiple comparisons with FDR correction.

(D) Representative images for data presented in (C). Only one representative condition is shown for neurons injected with the WT SARM1 construct. Survival of DsRed-positive neurons was assessed by comparing signal intensity and neuron size / shape at different timepoints, a method that provides an accurate reflection of survival rates (Gilley & Coleman, 2010).

Figure 6. R267W SARM1 decreases NAD^+ in transfected HEK cells as much as Δ226-232 SARM1.

(A) Relative levels of NAD^+ in extracts of HEK 293T cells 24 h after transfection with expression constructs for WT, R267W or Δ226-232 SARM1. 50 ng SARM1 vector was mixed with 750 ng empty vector for transfection (24-well plate format). NAD^+ levels are shown as a proportion of those in cells transfected with empty vector (ev) alone, performed in parallel. Means ±SEM with individual data points (n=6) are plotted. ***p<0.001 and n.s. = p>0.05, repeated measures multiple comparisons with FDR correction.

(B) Representative immunoblots of extracts as described in (A). Blots were probed as in Figure 2D. Four times the amount of extract and enhanced detection was needed to detect R267W and Δ226-232 SARM1 (bottom - the SARM1 band at ~70 kDa is indicated by an arrow, the additional band is non-specific). Like constitutively NADase hyperactive Δ226-232 SARM1, R267W SARM1 is expressed at a very low level but still causes substantial NAD^+ depletion and suppression of ZsGreen expression.

Variant	rsID	MAF [a]	Patients		Controls	
			Observed	*Expected*	**Observed**	*Expected*
Project MinE			*(4,366 ALS)*		*(1,832)*	
V112I	rs1032963037	0.000015	**1**	*0.13*	**0**	*0.05*
L223P	-	-	**1**	-	**0**	-
Δ226-232	rs782325355	0.000059	**2**	*0.51*	**0**	*0.22*
A240E	rs1449836804	0.000015	**1**	*0.13*	**0**	*0.05*
R244S	-	-	**1**	-	**0**	-
Δ249-252	-	-	**1**	-	**0**	-
A250T	rs1555585243	-	**1**	-	**0**	-
A275V	rs376587698	0.000029	**1**	*0.26*	**0**	*0.11*
A301S	rs782606059	0.00012	**3**	*1.03*	**0**	*0.43*
R310H	rs369186722	0.00016	**1**	*1.41*	**0**	*0.59*
V331E	rs1555585331	-	**1**	-	**0**	-
E340K	rs781854217	0.000059	**1**	*0.51*	**0**	*0.22*
A341V	rs373458416	0.00012	**2**	*1.03*	**0**	*0.43*
T385A	-	-	**1**	-	**0**	-
P332Q	rs140811640	0.012	**107**	*108.98*	**47**	*45.73*
N337D	rs375690432	0.00038	**3**	*3.34*	**1**	*1.40*
Answer ALS [b]			*(706 ALS)*		*(92)*	
Δ226-232	rs782325355	0.000059	**1**	*0.08*	**0**	*0.01*
R267W	rs11658194	0.000015	**1**	*0.02*	**0**	*0.00*
GENESIS [b]			*(1,984 ALS / HSP)*		*(11,602)*[c]	
Δ226-232	rs782325355	0.000059	**2** (1/1)	*0.23*	**0**	*1.36*

Table 1. SARM1 ARM domain coding variants in Project MinE and confirmed GoF alleles in other databases.

[a] MAF, minor allele frequency for European (non-Finnish) population in gnomAD v3.1.1.

[b] Only the GoF alleles identified in this study are reported for Answer ALS and GENESIS. Some of the relatively more common non-GoF alleles listed for Project MinE are present in these databases (A301S, A341V, P332Q and N337D).

[c] for the purposes of this study GENESIS controls are all the non-ALS and HSP patients in the database, although many have other disorders.

Clinical diagnosis (site of onset)	**SARM1 Variant**	Cohort	Sex	**Age-of-onset** / progression	Other variants	Close relatives affected
ALS (spinal)	**V112I**	Project MinE	M	**50-54** / 17 yr dead	None [b]	Not known
ALS (bulbar)	**L223P**	Project MinE	M	**55-59** / 3 yr dead	None [b]	Not known
ALS (bulbar)	**Δ226-232**	Answer ALS	F	**70-74** / 2 yr dead	None [c]	Not known
ALS	**Δ226-232**	GENESIS	M	**65-69** / 1 yr dead	*SOD1	None
ALS (spinal)	**Δ226-232**	Unattributed	F	**70-74** / 2 yr dead	Not available	None
ALS (spinal)	**Δ226-232**	Project MinE	M	**40-44** / 3 yr dead	None [b]	Not known
ALS (spinal)	**Δ226-232**	Project MinE	M	**55-59** / 3 yr dead	None [b]	Not known
ALS (bulbar)	**Δ249-252**	Project MinE	M	**65-69** / 4 yr dead	None [b]	Not known
ALS (spinal)	**R267W**	Answer ALS	M	**55-59** / 2 yr dead	**FIG4 [c]	Not known
ALS (spinal)	**V331E**	Project MinE	M	**50-54** / 5 yr dead	None [b]	Not known
ALS (spinal)	**E340K**	Project MinE	M	**75-79** / 6 yr dead	None [b]	Not known
ALS (spinal)	**T385A**	Project MinE	M	**65-69** / 6 yr alive	None [b]	Not known
HSP (pure)	**Δ226-232**	GENESIS	F	**5-9** / 14 yr alive	Not available	None
Upper and lower motor nerve disorder	**R267W**	UCL [a]	M	**40-44** / 25 yr alive	None [d]	None

Table 2. Clinical information for motor nerve disorder patients heterozygous for the Δ226-232 and R267W *SARM1* alleles.

*heterozygous for the partially-penetrant I114T *SOD1* variant associated with sporadic ALS

**heterozygous for the L17P *FIG4* variant, a variant that has previously only been associated with CMT4J in combination with a null allele.

[a] University College London, Queen's Square Institute of Neurology cohort.

[b] screened for variation in *C9orf72*, *FUS*, *SOD1* and *TARDBP.*

[c] screened for variation in *ALS2*, *ATXN2*, *C9orf72*, *CCNF*, *CHCHD10*, *FUS*, *OPTN*, *PFN1*, *SOD1*, *TARDBP*, *TBK1*, *UBQLN2*, *VAPB* and *VCP.*

[d] screened for variation in *Androgen Receptor* expansion, *ALS2*, *ANG*, *C9orf72*, *CYP7B1*, *DCTN1*, *FA2H*, *FIG4*, *FUS*, *GJC2*, *KIAA0196*, *KIF5A*, *NIPA1*, *OPTN*, *PLP1*, *PNPLA6*, *REEP1*, *RTN2*, *SPAST*, *SPG7*, *SLC52A1*, *SLC52A2*, *SLC52A3*, *SMN*, *SOD1*, *TARDBP*, *UBQLN2*, *VAPB*, *VCP*, whole mtDNA sequencing in blood.

Figure 1

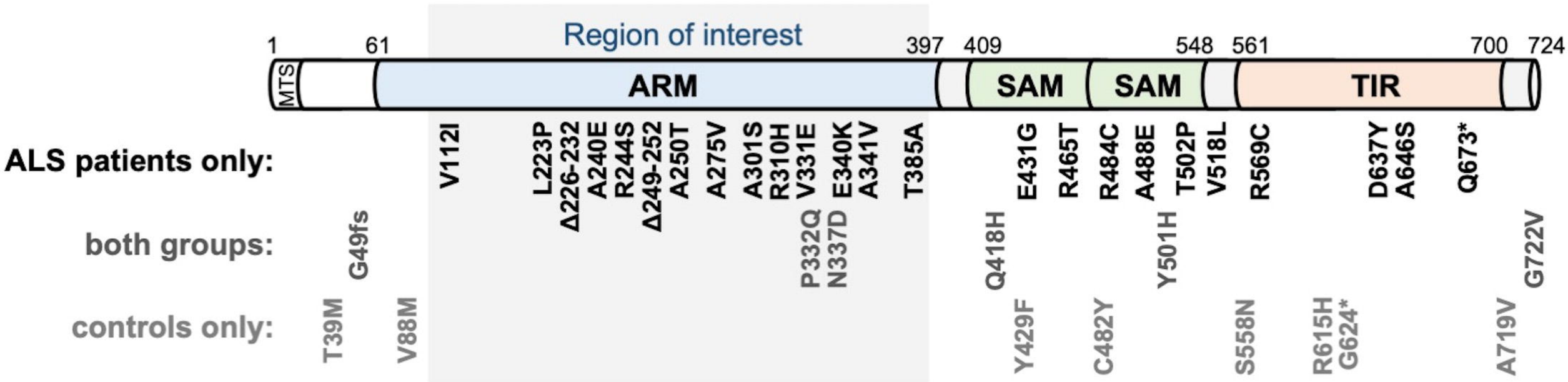

Figure 2

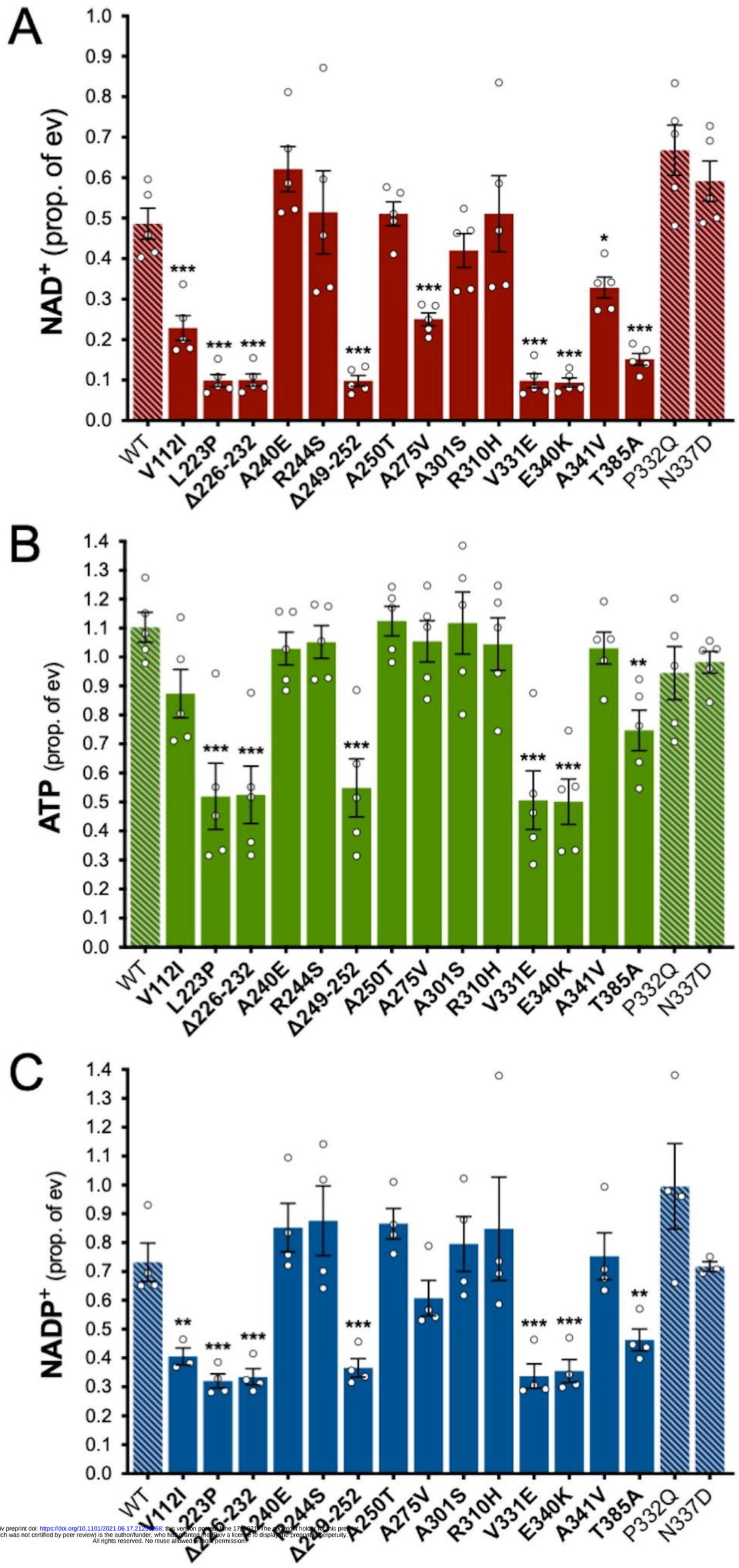

Figure 3

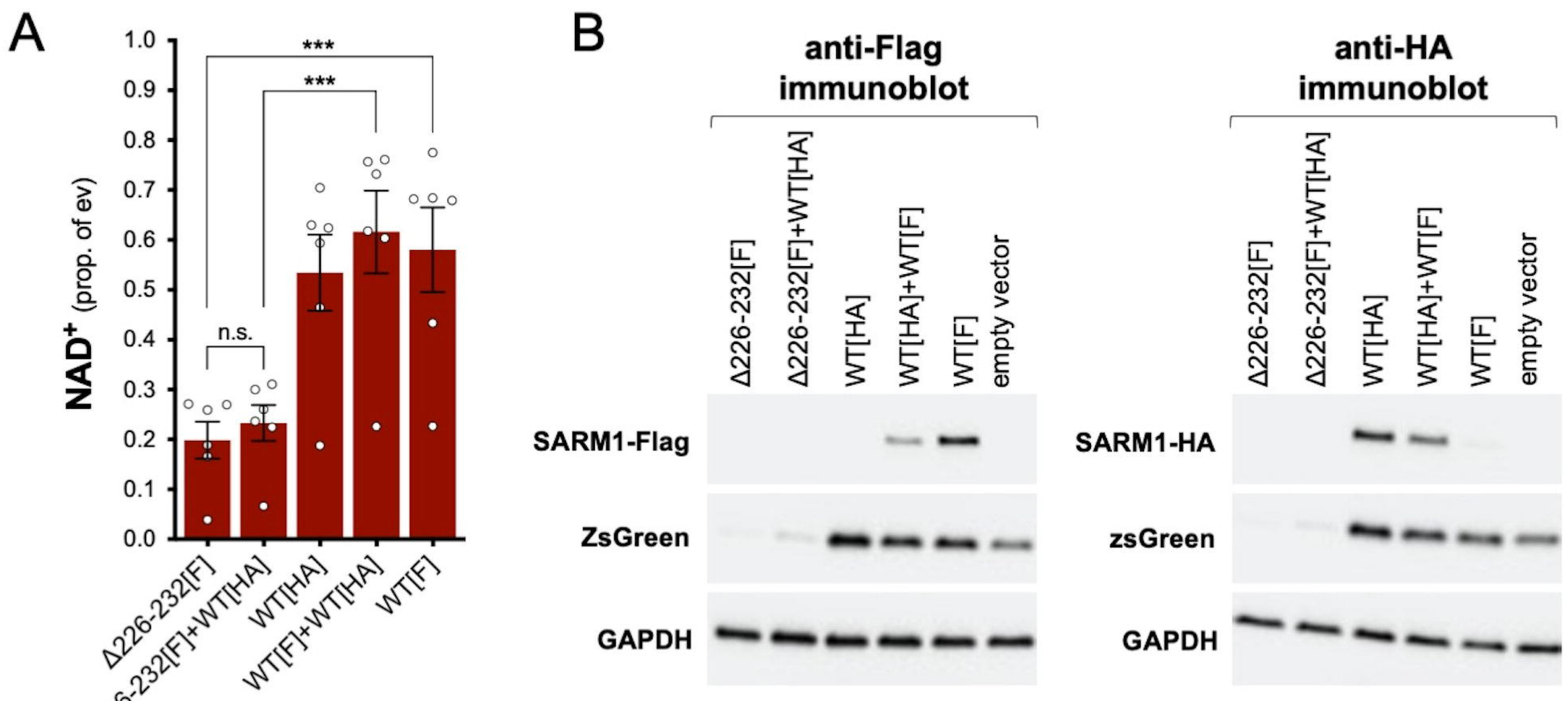

Figure 4

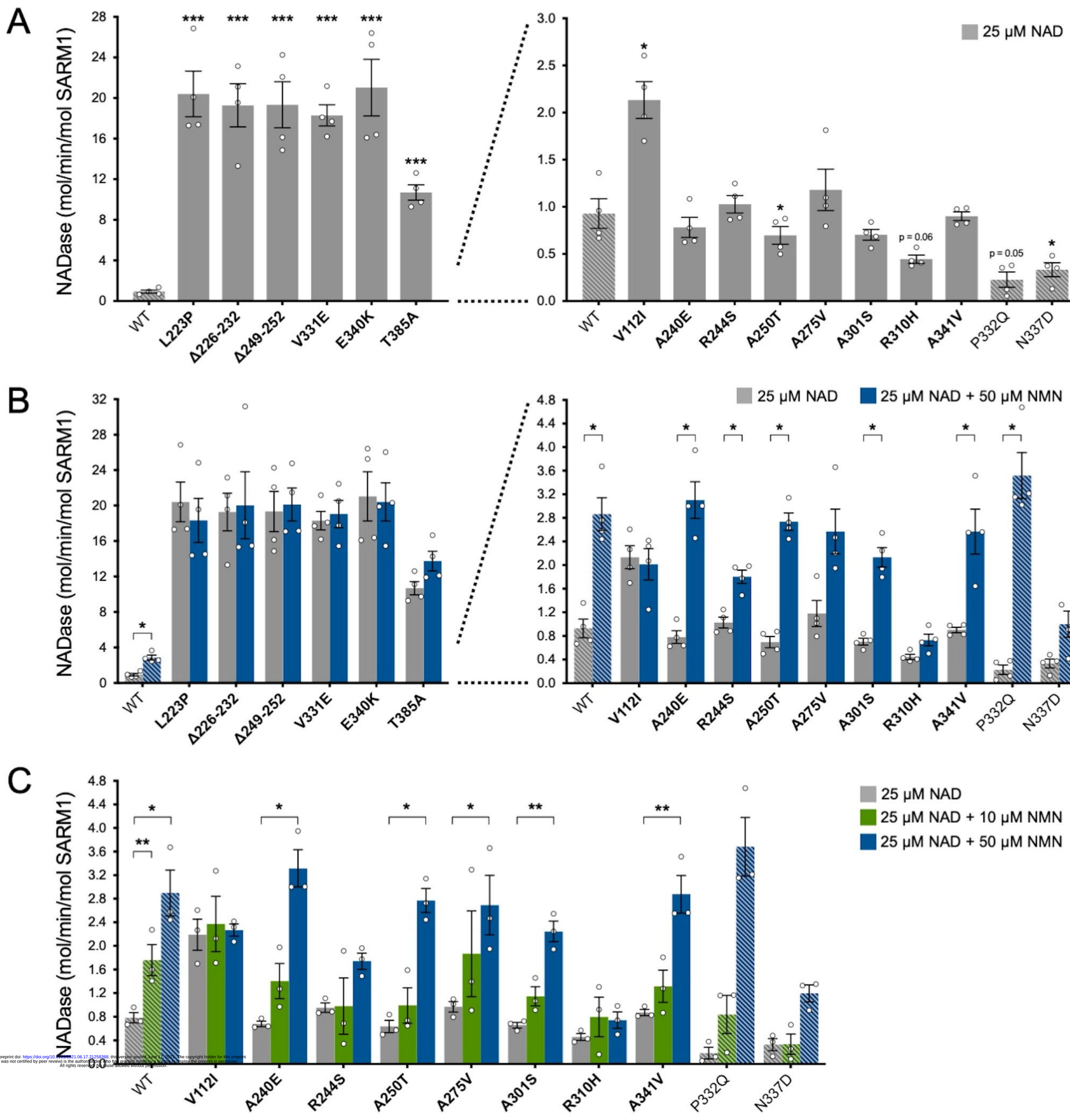

Figure 5

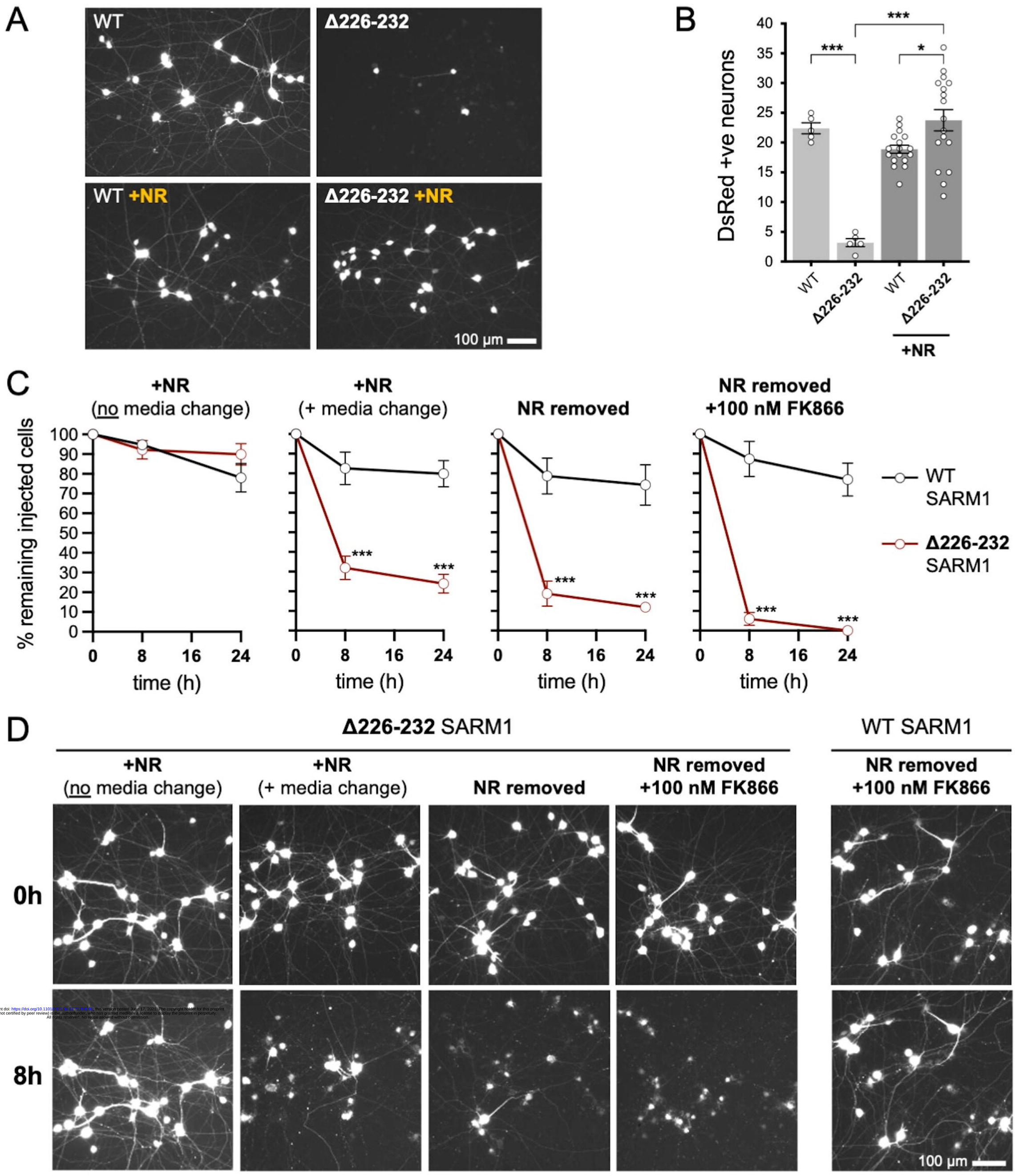

Figure 6